

Review

Recent advancement and key opportunities of MXenes for electrocatalysis

Xianhong Wu,^{1,2} Yi Wang,^{1,4} and Zhong-Shuai Wu^{1,3,*}

SUMMARY

MXenes are promising materials for electrocatalysis due to their excellent metallic conductivity, hydrophilicity, high specific surface area, and excellent electrochemical properties. Herein, we summarize the recent advancement of MXene-based materials for electrocatalysis and highlight their key challenges and opportunities. In particular, this review emphasizes on the major design principles of MXene-based electrocatalysts, including (1) coupling MXene with active materials or heteroatomic doping to create highly active synergistic catalyst sites; (2) construction of 3D MXene structure or introducing interlayer spacers to increase active areas and form fast mass-charge transfer channel; and (3) protecting edge of MXene or *in situ* transforming the surface of MXene to stable active substance that inhibits the oxidation of MXene and then enhances the stability. Consequently, MXene-based materials exhibit outstanding performance for a variety of electrocatalytic reactions. Finally, the key challenges and promising prospects of the practical applications of MXene-based electrocatalysts are briefly proposed.

INTRODUCTION

With ever-increasing concerns of environmental pollution and global energy crisis,¹ developing sustainable clean energy is becoming more and more important in our world; in particular, electricity can be coupled with clean energy sources such as wind, tidal, and solar power. Electrocatalytic conversion can effectively use renewable resources to produce clean energy. For example, water splitting can produce hydrogen.² Carbon dioxide reduction reaction (CO₂RR) can reduce the emission of greenhouse gas and produce CO, CH₄, formate, etc.³ Electrocatalytic conversion reactions are also the key reaction in the production of fuel cells.⁴ Therefore, developing electrocatalysts with high activity and long life is crucial to unleash the potential of electrocatalytic conversion reaction and realize industrial production.⁵

MXenes, a new key family of two-dimensional (2D) transition metal carbides, nitrides, boride, and carbonitrides, were discovered by Naguib et al. in 2011.^{6,7} MXenes are usually synthesized by selectively etching out the A layers from the MAX phase (M_{n+1}AX_n), where M represents transition metal (M = Sc, Ti, V, Cr, Zr, Nb, Mo, Hf, Ta), A represents group IIIA or IVA element (such as Al, Ga, Si, or Ge), and X represents C, N, and/or B element.⁸ During the usually etching process in HF or HCl/LiF solution,⁹ there are abundant surface functional groups on the surface of MXenes, including -O, -OH, and -F. As a result, MXene is usually written as M_{n+1}X_nT_x, where T is the surface functional group. Up to date, there are a variety of MXenes, including Ti₃C₂T_x,⁷ Ti₂CT_x,¹⁰ Ti₄N₃T_x,¹¹ Mo₂CT_x,¹² Nb₂CT_x,¹³ (Nb_{0.8}Ti_{0.2})₄C₃T_x,¹⁴ (Nb_{0.8}Zr_{0.2})₄C₃T_x,¹⁴ V₂CT_x,¹⁵ and Mo_{4/3}B_{2-x}T_x,¹⁶ that have been synthesized, and more types of MXenes have been predicted according to theoretical calculations.¹⁷

Due to the fascinating properties of MXene, research on MXenes for electrocatalysis has caused a veritable of interest.^{18–20} (1) The high conductivity (6,000–8,000 S cm⁻¹) of MXene can facilitate the fast transport of electrons.^{21,22} (2) Abundant adjustable surface functional groups give it excellent hydrophilicity, which promotes the infiltration of the electrolyte and contributes to the adsorption of reactive species in water electrolysis reaction.^{23,24} (3) The abundant surface functional groups make MXene easily coupled with other compounds to form new synergistic catalytic sites.²⁵ (4) The rich composition makes the catalytic properties of MXene adjustable.²⁶ (5) 2D structure enables it abundant active sites and short mass-charge transport paths.^{27,28} And (6) the low work function and electronegative surface of MXene endow it excellent carrier material, which can regulate the electronic structure of active center. However, there are some key challenges for MXenes in electrocatalysis, such as easy restacking, limited intrinsic catalytic activity, and poor stability at oxygen atmosphere. Recently, many key strategies have been reported to improve their catalytic activity (**Scheme 1**). The typical strategies to enhance the catalytic activity of MXenes include the following: (1) The introduction of interlayer spacers to prevent MXenes stacking and construction of three-dimensional (3D) MXenes structure is conducive to the exposure of catalytic surface, increasing the amount of catalyst active sites. (2) The MXene-based catalyst with high intrinsic catalytic activity can be designed by doping heteroatom and coupling with other active materials. And (3) oxidation of MXenes can be refrained by avoiding exposure of the edge sites of MXenes to oxygen or *in situ* conversion of the surface of MXenes to stable substances. As a

¹State Key Laboratory of Catalysis, Dalian Institute of Chemical Physics, Chinese Academy of Sciences, Dalian 116023, China

²College of Light Industry and Chemical Engineering, Dalian Polytechnic University, Dalian 116034, China

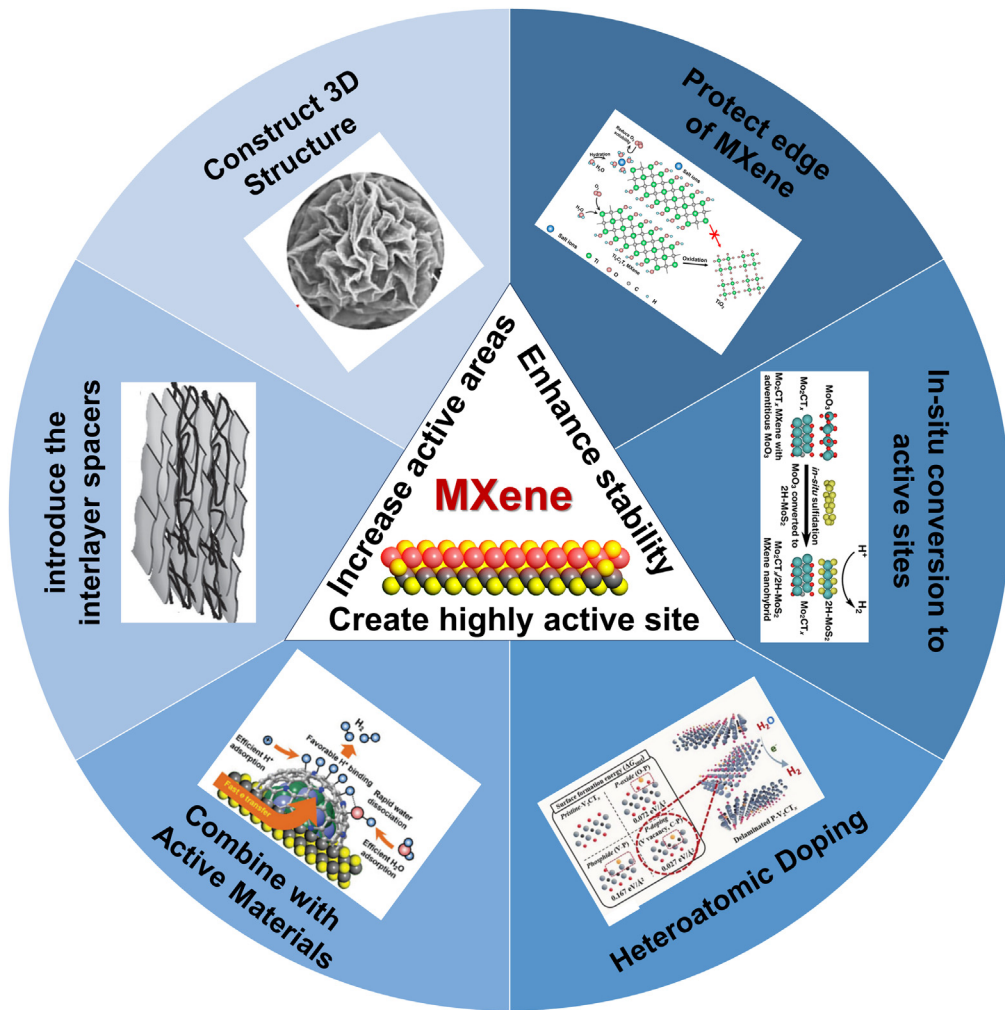
³Dalian National Laboratory for Clean Energy, Chinese Academy of Sciences, Dalian 116023, China

⁴University of Chinese Academy of Sciences, Shijingshan District, Beijing 100049, China

*Correspondence: wuzs@dicp.ac.cn

<https://doi.org/10.1016/j.isci.2024.108906>





Scheme 1. The key strategies of designing MXene-based electrocatalysts

result, MXene-based catalysts possess large specific surface area, excellent conductivity, hydrophilicity, stability, and intrinsic catalytic activity, which is highly beneficial to develop robust electrocatalysts with high catalytic activity and long-term durability.

STRUCTURAL CHARACTERISTICS AND PROPERTIES OF MXenes

Similar to the MAX phase precursors, the crystalline phase of MXenes possesses a hexagonal tightly packed structure with X atoms arranged in the body center of MXenes octahedrons. The transition metal atoms are located in tightly packed structure in MXenes, whereas the nonmetal atoms are packed in the octahedral interstitial positions.²⁹ Consequently, most MXenes are highly conducting. For example, pure $\text{Ti}_3\text{C}_2\text{T}_x$ shows high electrical conductivities of $2.4 \times 10^5 \text{ S m}^{-1}$,²¹ which is an important performance parameter in energy storage and conversion. The density of free carries of MXenes is also relatively high, e.g., $8 \pm 3 \times 10^{21} \text{ cm}^{-3}$ of $\text{Ti}_3\text{C}_2\text{T}_x$,³⁰ and $3 \times 10^{20} \text{ cm}^{-3}$ of Mo_2CT_x ,³¹ and the work function of MXenes is relatively low, e.g., $3.9\text{--}4.8 \text{ eV}$ of $\text{Ti}_3\text{C}_2\text{T}_x$,³² which can enhance charge transfer kinetics.

Usually, HF or LiF/HCl mixed solution is used to etch A component of MAX, thus the surface of MXenes has rich -OH, -F, and -O surface functional groups, which can allow strong interfacial coupling of the ions, thereby facilitating the intercalation of cations and combination with compounds. Moreover, the surface functional group can also render the MXenes' high hydrophilicity (water contact angle of $21.5\text{--}35^\circ$), which is conducive to be used in advanced electrocatalyst.¹⁰ What is more, the large specific surface area and highly open structure inherited from their 2D structure also make MXenes promising for electrocatalysis.^{5,30,33} MXenes also shows excellent mechanical properties, e.g., the tensile strengths of a $\sim 3.3\text{-}\mu\text{m}$ -thick $\text{Ti}_3\text{C}_2\text{T}_x$ film was $22 \pm 2 \text{ MPa}$, with Young's modules of $3.5 \pm 0.01 \text{ GPa}$.²¹ And the strength of $\text{Ti}_3\text{C}_2\text{T}_x/\text{PVA}$ film was further improved to $91 \pm 10 \text{ MPa}$. By mixing $\text{Ti}_3\text{C}_2\text{T}_x$ film with thermoplastic polyurethane, the tensile strength and elongation at break could rise by 41.2% and 15.4%, respectively.³⁴ The outstanding mechanical properties promote the structural diversity and stability of MXene-based electrocatalyst.

DESIGN STRATEGY OF MXENE-BASED CATALYST

Increase catalytic active sites

For electrocatalysis, the number of active sites is an important factor in determining electrocatalytic activity. However, MXene layers tend to restack, due to the electrostatic force between the adjacent layers, which hinders the transport of electrolyte ions and limits the full utilization of their surfaces. One effective strategy to inhibit the stacking of 2D materials and improve their electrocatalytic performance is to introduce the interlayer spacers between MXene layers, including the nanoparticles (NPs),³⁵ nanotubes/nanowires,³⁶ and 2D nanosheets.³⁷ In another way, the interlayer spacing of MXenes could increase after intercalating cetyltrimethylammonium bromide and stearyltrimethylammonium bromide pillars.³⁵

Processing MXenes to hierarchical 3D architecture, such as porous films, scaffolds, and networks, is another key strategy to resist the aggregation, which can increase the specific surface area, preserve the intrinsic properties of MXenes, and render the additional characteristics such as fast mass-charge transfer channels, high robustness, and processability. The 3D MXene architecture can be prepared by ultrasonic-assisted aerosol spray drying³⁸; sacrificial poly(methyl methacrylate) spherical templates³⁹; assembly of MXene/rGO aerogel,^{40–43} MXene/polyimide aerogel,⁴⁴ and MXene aerogel^{45–47}; and 3D printing.⁴⁸ For instance, Zhao et al. reported an effective method of electrostatic self-assembly that can assemble 2D MXene nanosheets with negatively charged and 2D layered double hydroxides (LDH) with positively charged into 3D hollow structure.⁶ Similarly, Xiao et al. reported the flower-like porous $Ti_3C_2T_x$ by the presence of ethanediamine.⁴⁹ These results indicated that assembling MXenes into 3D porous and hollow structure was an effective means to enhance the electrochemical performance, which could improve the diffusion and permeation of electrolytes. Further, chemical etching such as acid/alkali treatment⁵⁰ and catalytic oxidation of MXenes flakes using transition metal salt⁵¹ were also the effective ways to prepare porous MXenes. Besides, the deposition of MXenes on 3D integral, e.g., nickel foam (NF), was also a feasible means to maintain its high active area and construct 3D porous skeleton structure for electrolysis directly.^{52,53}

Heteroatomic doping of MXenes

Heteroatomic doping of MXenes can improve the electrochemical performance by providing new active site, changing the electronic structure of MXenes, and affecting the adsorption capacity.^{54–56} Typically, Yoon et al. reported an effective strategy to improve catalytic activity of MXene for hydrogen evolution reaction (HER) by interfacial chemical doping with a nonmetallic P, which was an electron donor. Thus, the P-C bonds in $P\text{-}V_2CT_x$ could work as active sites, which balanced the energy barriers of H^+ reduction and H_{ads} desorption well, enhancing the kinetics of HER.⁵⁴ Further, Kuznetsov et al. reported a $Mo_2CT_x\text{:Co}$ phase that was obtained from $Mo_2Ga_2C\text{:Co}$, which greatly improved HER activity. It is calculated that the hydrogen adsorption energy on the MXene surface was significantly improved after Co doping.⁵⁷

Surface modification of MXenes for electrocatalyst

MXenes are an excellent electrocatalytic platform material to design and synthesize high-activity electrocatalyst by *in situ* growth of catalytic active materials on their surface, thanks to the abundant surface functional groups, excellent hydrophilicity, high surface activity, and conductivity.^{33,58,59} First, MXene is beneficial to act as the active substance to expose more active sites. Second, it can increase the hydrophilicity of the material and promote the initial adsorption of the active species for water splitting. Third, MXene-based catalyst material can be endowed with high conductivity, accelerating the transport of electrons. Further, the strong interaction between MXene and the active substance can intrinsically optimize the electronic structure of active center, boosting the catalytic activity, such as $C_3N_4\text{/Ti}_2C_3$,⁶⁰ $Ti_3C_2T_x\text{-Co}$ 1,4-benzene-dicarboxylate,⁶¹ and $Co(OH)_2\text{@MXene}$.⁶² Last but not the least, new high-activity site can be formed by bonding MXenes with active substance. For example, the catalyst containing $FeN_3O\text{-O-Ti}$ could be synthesized by coupling Fe-chelated polymer-like quantum dots with ultrathin O-terminated MXenes ($Ti_3C_2O_x$), enhancing oxygen reduction reaction performance.⁴ Besides, Pt_3Ti alloy was formed on the surface of $Ti_3C_2T_x$ MXene, showing high activity for HER.⁶³

What is more, MXenes are ideal platform materials for preparing single-atom catalysts. (1) Single atom can be uniformly anchored to the defect sites on the surface of MXenes. For instance, the Mo vacancies on the surface of $Mo_2TiC_2T_x$ MXene can act as the anchoring sites for single Pt atom for HER.⁶⁴ (2) Via introducing non-metallic elements (e.g., N, S, P) on the surface of MXenes, single atom can be anchored on the surface of MXenes by bonding between non-metallic elements and metallic single atom. In this regard, non-metallic elements can also be used to efficiently regulate the electronic structure of single atom to improve catalytic activity. Representative, $Ru_{SA}\text{-N-S-Ti}_3C_2T_x$ catalyst showed excellent HER performance.⁶⁵ (3) The composition of MAX phase is rich and adjustable so that single-atom catalysts on MXenes can be prepared by changing the composition of A and choosing a suitable selective etching method. For example, a single-atom Cu-MXene catalyst can be obtained by selective etching of Al from $Ti_3(Al_{1-x}Cu_x)C_2$.³

Improves durability of MXenes

With a high-proportion exposure of metal atoms on the surface of MXenes, the MXenes are usually thermodynamically metastable with high surface energy, suffering from poor oxygen tolerance.^{22,66–69} Therefore, it is of great importance to prevent the oxidation of MXene so that its structure and properties can be preserved, its preservation time can be extended, and it can undergo high temperature reaction. For instance, a simple carbon coating strategy has been developed to stabilize MXenes against structural collapse caused by spontaneous oxidation.²² Further, it has been reported that adding high-concentration nontoxic inorganic salts, such as $NaCl$, $LiCl$, and $CaCl_2$, in MXenes dispersion can inhibit the oxidation of MXenes. The hydration effect of inorganic salts could reduce the ratio of free water molecules in the MXenes

dispersion, restricting the oxygen solubility simultaneously, which suppresses MXenes oxidation.⁷⁰ Similarly, the V₂CT_x flakes were assembled by Li⁺ cations (Li-V₂CT_x), appear to be much stability,⁷¹ and capping the edge of MXenes sheets with polyanionic salt could slow down the oxidation process even in aerated water.⁷² Further, Zhao et al. reported that sodium L-ascorbate could protect the edges of the MXenes, restricting water molecules from otherwise reactive sites.⁷³ It is suggested that covering the edge of MXenes with other molecules can prevent its oxidation effectively. Other methods have been reported, such as hydrogen annealing⁷⁴ and freezing aqueous MXenes dispersions at a low temperature.⁷⁵

In another way, the surface oxidation products of MXene can be used as active materials.^{76,77} As exemplified, Tang et al. developed a controlled anodic oxidation method to improve the rare performance of Ti₃C₂T_x MXene in acidic electrolyte for pseudocapacitive energy storage.⁷⁸ Our group reported the designed fabrication of nanoribbons of sodium-titanate (NaTi_{1.5}O_{8.3}) and potassium titanate (K₂Ti₄O₉) for sodium/potassium ion batteries by oxidation and alkalinization process of Ti₃C₂ MXene.⁷⁹ Later, Fang et al. reported a one-step ethanol thermal oxidation method to *in situ* convert surface of Ti₃C₂T_x MXene to oxygen-vacancy-rich TiO₂, where the oxygen vacancies worked as the active sites for nitrogen reduction reaction (NRR).⁷⁶ Meanwhile, the TiO₂ of TiO₂-MXene (Ti₃C₂T_x) heterostructures could promote the adsorption and conversion activity of polysulfides in lithium-sulfur batteries.⁸⁰ Significantly, Yury et al. developed a strategy to avoid the oxidation of Mo₂CT_x/MXenes by *in situ* vulcanizing surface of Mo₂CT_x MXene to form Mo₂CT_x/2H-MoS₂ hybrid structure. The tight coupling between the Mo₂CT_x and 2H-MoS₂ interface guaranteed fast mass-charge transfer, then exhibiting superior HER activities.⁷⁷

Applications in electrocatalysis

MXenes are considered as potential electrocatalytic material, thanks to their excellent electrical conductivity, hydrophilicity, high surface activity, low work function, and electronegative, which accelerates the transport of electrons, promotes the infiltration of electrolyte, and regulates the electronic structure of active center. As a consequence, MXene-based materials have been developed for various electrocatalysis.

MXene-based materials for oxygen reduction reaction

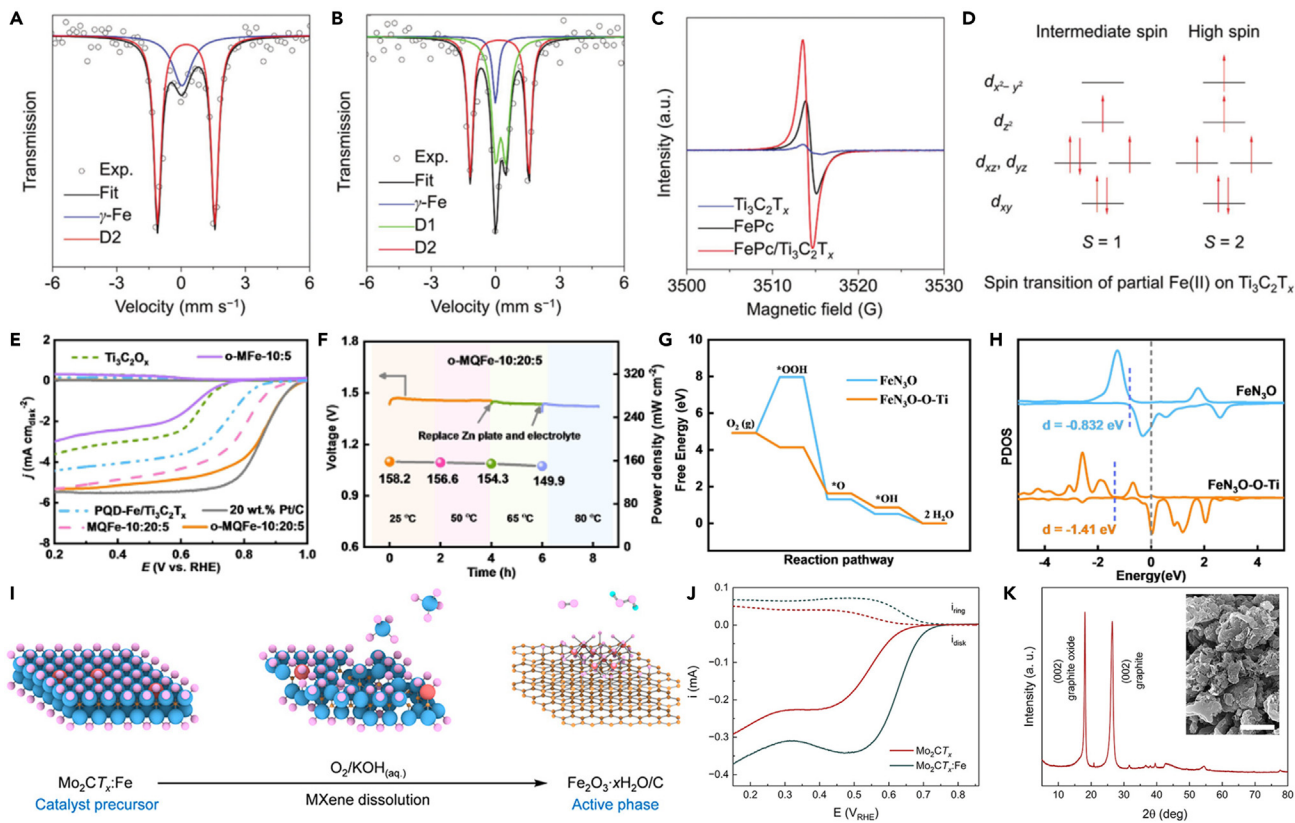
The oxygen reduction reaction (ORR) is one of the crucial processes in many renewable energy application, including metal-air batteries and fuel cells.⁸¹ To meet the needs of practical applications, the development of electrocatalysts with high catalyst activity and long durability has been urgently needed. To this purpose, by combining catalytic active materials and MXenes, the electron density distribution of catalyst active centers can be remarkably enhanced, and new active sites would appear.

MXenes can be used to readily regulate the electronic structure or change the bonding state of the catalytic activity center to promote catalytic activity in ORR. For instance, the ORR activity of catalyst could be enhanced by coupling FeN₄ and Ti₃C₂T_x MXene, due to the formation of Fe-N-C active sites.⁸² The binding of FeN₄ and MXene could lead to significant Fe 3d electron delocalization and spin-state transition of Fe(II) ions. Then the lower local electron density and higher spin state of the Fe(II) centers significantly favored electron transfer of Fe d_{2z}, making it easier for oxygen adsorption and reduction at FeN₄ active center, thereby improving electrocatalytic activity of ORR (**Schemes 2A–2D**). In addition, Wang et al. coupled Fe-chelated polymer-like quantum dots with Ti₃C₂O_x MXene, called o-MQFe, to form Fe-O-Ti ligand, which adjust the spin state transition of Fe, thus enhancing the electrocatalytic activity of ORR.⁴ Compared with the contrast catalysts without Fe-O-Ti ligand, the intrinsic electrocatalytic activity for ORR of o-MQFe was significantly improved, exceeding the commercial Pt/C catalyst (**Scheme 2E**). Furthermore, Zin-air batteries and H₂/O₂ fuel cell systems based on o-MQFe catalyst achieved outstanding performance in a wide temperature (**Scheme 2F**). Further, it is theoretically calculated that Fe-O-Ti ligands in FeN₃O-O-Ti could lead to a low-to-medium spin-state transition and optimal oxygen adsorption energy (**Schemes 2G** and **2H**). What is more, Wang et al. reported that the Ti₃C₂ MXene could be used to stabilize molecularly thin nitride sheets of NiFeMn trimetallic nitride.⁸³ The strong interaction between metallic Ti₃C₂ MXene sheets and nitrides could promote charge transport redistribution. In addition, the M–N–C or M–N–Ti ligands could be obtained at the interface, which brought about an outstanding electrocatalytic activity of ORR. It is indicated that MXene coupled with electrochemically active materials can produce new active sites with high catalytic activity for ORR. The abovementioned results showed that the electronic structure and electronic spin mode of Fe could be changed when coupled with MXene, due to the strong interaction between MXene and Fe, thereby increasing the ORR activity.

Interestingly, Muller et al. reported Mo₂CT_x MXene nanosheet with single-atomic iron sites (Mo₂CT_x:Fe), which showed high catalytic activity for ORR and selective oxygen reduction to hydrogen peroxide.⁸⁴ However, the Mo₂CT_x:Fe transformed *in situ* into a graphitic carbon framework with dispersed iron oxyhydroxide (ferrihydrite, Fh) species (Fh/C) after the catalytic tests, which were the actual active species. Because the metal atoms of MXene are easily decomposed in alkaline environment containing oxygen, it is highly necessary to characterize the *in situ* reconstruction process of MXene during electrocatalysis to determine the actual catalytic active site.

MXene-based materials for oxygen evolution reaction

The oxygen evolution reaction (OER) is the cornerstone for many electrocatalytic application, including electrochemical water splitting, fuel cells, and metal-air batteries.⁶¹ MXene-based materials also have many applications for OER. For example, 2D Ti₃C₂ MXene nanosheets were coupled with 2D g-C₃N₄ via Ti-N_x interaction, which formed a porous free-standing film with high hydrophilic surface and conductive frame (**Scheme 3A**), thus showing outstanding catalytic activity of OER.⁶⁰ Except mechanically mixing, 2D materials could be grown on the surface of MXene. As exemplified, Wang et al. validated the fabrication of NiFe-LDH on the surface of MXene for OER.⁸⁵ The charge analysis showed that there was a 0.09e per unit cell from FeNi-LDH to MXene, indicating the close relationship between FeNi-LDH and MXene (**Scheme 3B**). The strong interfacial electron interaction between MXene and LDH not only guaranteed fast conductivity and robust structure of the



Scheme 2. MXene-based materials for ORR

(A and B) Fe Mössbauer transmission spectra and their deconvolution of pristine FePc and $\text{FePc}/\text{Ti}_3\text{C}_2\text{T}_x$.

(C) X-band ESR spectra of pristine $\text{Ti}_3\text{C}_2\text{T}_x$, FePc, and $\text{FePc}/\text{Ti}_3\text{C}_2\text{T}_x$.

(D) Schematic representation of the spin transition of partial Fe(II) on $\text{Ti}_3\text{C}_2\text{T}_x$.⁸² Copyright 2018 WILEY-VCH Verlag GmbH & Co. KGaA, Weinheim.

(E) LSV curves of different catalysts.

(F) The open-circuit voltage and peak power density at different temperatures.

(G) The free energy changes for ORR and (H) the PDOS of Fe 3d orbital for FeN_3O and $\text{FeN}_3\text{O-O-Ti}$. The blue dotted lines denote the d-band centers, while the gray dotted line denotes the Fermi level.⁴ Copyright 2022 Wiley-VCH GmbH.

(I) *In situ* reconstruction of $\text{Mo}_2\text{CT}_x:\text{Fe}$ catalyst during reaction.

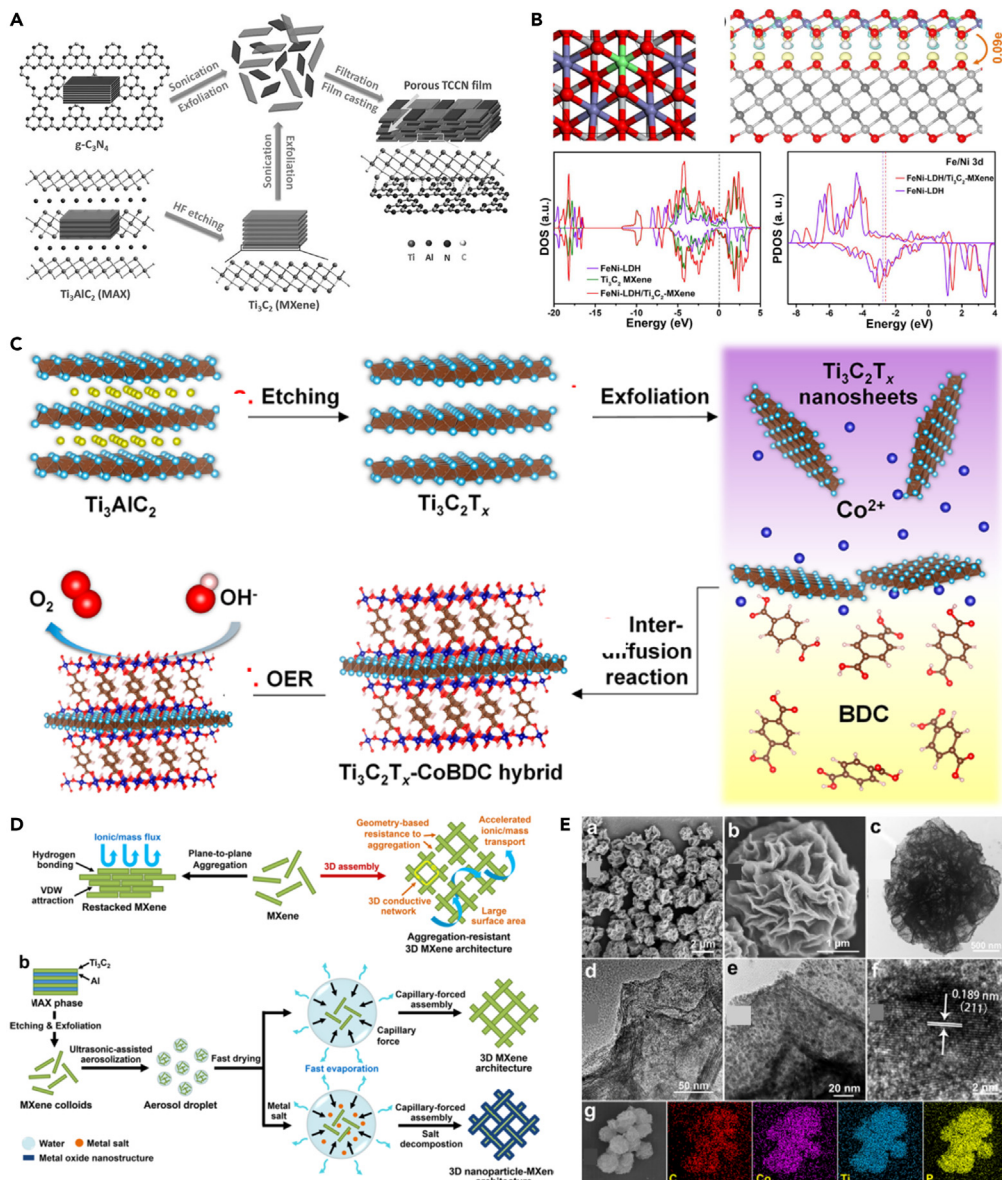
(J) Anodic-going polarization curves for the electrodes with deposited $\text{Mo}_2\text{CT}_x:\text{Fe}$ or Mo_2CT_x .

(K) XRD patterns of Fh/C that indicate the presence of graphite and graphite oxide phases. The inset shows a SEM image of the Fh/C material (the scale bar is 1 μm).⁸⁴ Copyright 2021 American Chemical Society

nanohybrid but also accelerated the electrocatalytic process of FeNi-LDH in the OER. It is demonstrated that different 2D materials could be coupled through the interactions to improve their catalytic activity due to the strong interaction.

In addition to coupling with 2D materials, MXene can also be married with MOF to construct high active catalytic sites. Recently, Huang et al. reported the synthesis of a MXene-MOF composite, $\text{Ti}_3\text{C}_2\text{T}_x$ -cobalt 1,4-benzenedicarboxylate ($\text{Ti}_3\text{C}_2\text{T}_x\text{-CoBDC}$), showing excellent electrocatalytic OER activity (Scheme 3C).⁶¹ In the electrocatalyst process, the well-defined interface between $\text{Ti}_3\text{C}_2\text{T}_x\text{-CoBDC}$ promotes fast charge and ion transfer. Additionally, the $\text{Ti}_3\text{C}_2\text{T}_x$ nanosheets with high hydrophilicity could prevent the aggregation of porous CoBDC MOF layers and make the aqueous electrolyte easy to approach the electrocatalyst surface, thus resulting in high electrocatalytic activity for OER. Further, MXene can also be coupled with the NPs to construct highly active composite materials. For instance, it is reported that Co NPs coated with nitrogen-doped multiwalled CNTs were grown on the surface of $\text{Ti}_3\text{C}_2\text{T}_x$ MXene (Co/N-CNTs@ $\text{Ti}_3\text{C}_2\text{T}_x$) as bifunctional electrocatalyst for ORR and OER.⁸⁶ The abovementioned results show that MXene can interact with active substances to modulate the electronic structure of active center, create new active sites, then enhance the catalytic activity of the resulting catalysts. Meanwhile, MXenes can be used as excellent platform materials for electrocatalyst due to its high conductivity and hydrophilicity.

Significantly, 2D MXene can form 3D structure to avoid the restacking between the adjacent layers and then improve the electrocatalytic activity by increasing catalytic active sites and fast charge-mass transport channel. For instance, Wang et al. assembled 2D Ti_3C_2 MXene into hierarchical 3D architecture using ultrasonic-assisted aerosol spray drying of MXene colloids (Schemes 3D and 3E).³⁸ As a consequence, the 3D MXene structure possessed larger specific surface area, 3D conductive frame, and excellent processability. Importantly, synergistically coupling 3D MXenes with electrocatalytic active materials could yield new composite materials with abundant active sites, fast mass-charge



Scheme 3. MXene-based materials for OER

(A) Fabrication of the porous Ti₃C₂-C₃N₄ film.⁶⁰ Copyright 2016 Wiley-VCH Verlag GmbH & Co. KGaA, Weinheim.

(B) Model structure, density of states (DOS), and projected DOS of FeNi-LDH/Ti₃C₂-MXene.⁸⁵ Copyright 2017 Elsevier Ltd.

(C) Schematic illustration of the preparation process of Ti₃C₂T_x-CoBDC hybrid for OER.⁵¹ Copyright 2017 American Chemical Society.

(D) Capillary-forced assembly of MXene into 3D architecture by spray drying the aerosol droplet of MXene-containing colloids and its application for OER.

(E) SEM, TEM, HRTEM and elemental mapping of CoP@3D Ti₃C₂-MXene architecture.³⁸ Copyright 2018 American Chemical Society.

transport channels, and excellent intrinsic catalytic activity. Specifically, CoP@3D Ti₃C₂-MXene composite material showed higher electrocatalytic activity than CoP@2D Ti₃C₂-MXene and MXene-free CoP for OER and HER. It is noted that MXene could not only be self-assembled into 3D structures but also be constructed into 3D structures with the help of other 3D skeletons. As demonstrated, this group also reported a strategy for utilizing 3D MXene framework as structural scaffold for water-splitting by coupling NiFe-LDH nanosheets with 3D MXene framework of a microporous NF scaffold.²⁴ It is suggested that the 3D MXene framework with large surface area, high conductivity, reactivity, and hydrophilicity could enhance the charge transfer kinetics and adsorption/activation of the water molecules, thus promoting the OER.

MXene-based electrocatalysts showed excellent catalytic activity for OER. However, the instability of MXene in OER is still difficult to be overcome. MXene, including V₂CT_x, Ti₃C₂T_x, and Mo₂CT_x, will be oxidized in KOH at high oxidation voltage.^{5,84,87} Thus, the dynamic changes of catalyst during OER should be characterized to determine the true activity site and guide the design of the MXene-based materials, further improving the activity and stability.

MXene-based materials for hydrogen evolution reaction

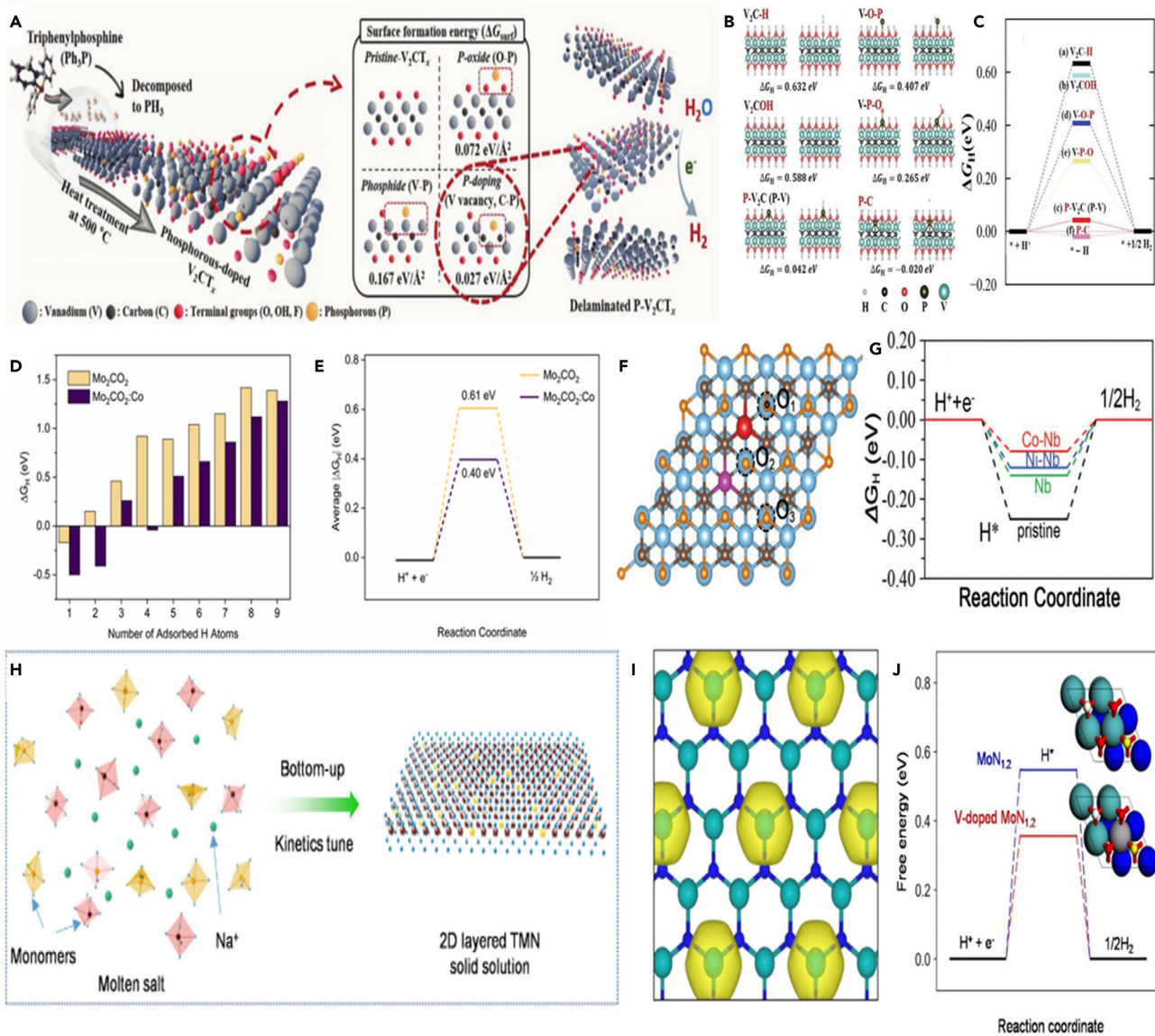
Water electrolysis is considered to be one of the most economical and cleanest methods for hydrogen production.⁸⁸ However, lack of cheap, high-activity, and long-life electrocatalysts has limited the rapid development of this technology.² To this end, MXenes can be used as promising electrocatalyst for HER due to their outstanding physical and chemical properties, including high conductivity, hydrophilicity, reactivity, rich composition, and adjustable surface functional groups.

Heteroatomic doping of MXenes is also an effective method to enhance the catalytic activity by optimizing electronic structure of the active center or providing new high active sites.^{54,89} For instance, the activity of 2D V₂CT_x MXene has improved after P-element doping (**Scheme 4A**).⁵⁴ It is calculated that the P-C bonding showed the lower surface formation energy (ΔG_{Surf}) of 0.027 eV Å⁻² and Gibbs free energy (ΔG_H) of -0.02 eV (**Scheme 4B**). The P-V₂CT_x treated at 500°C showed a higher P-C bond concentration with a smaller overpotential of -163 mV to achieve a current density of 10 mA cm⁻² ($\eta_j = 10$). It is evidenced that the P-C bonds in P-V₂CT_x could act as the active center, which results in hydrogen binding energy close to zero, balancing the energy barriers of H⁺ reduction and H_{ads} desorption, then improving HER activity (**Scheme 4C**). In addition to the doping of nonmetallic element, the doping of metallic elements can also improve the HER activity of MXene. For example, Kuznetsov et al. fabricated Co-doped molybdenum carbide (β -Mo₂C:Co) from Mo₂CT_x:Co phase.⁵⁷ It is calculated that the thermodynamics of hydrogen biding on the MXene surface has improved after Co coped, which improves the HER activity (**Schemes 4D and 4E**). Further, Du et al. synthesized NiCo alloy anchored on Nb-doped Ti₃C₂T_x MXene (named as NiCo@NTM) as HER electrocatalyst.⁵⁵ It is calculated that the Nb doping could move the Fermi energy level up to the conduction band, thereby improving the electronic conductivity. In addition, the Co-Nb site displayed the more suitable hydrogen binding energy, close to zero, which further enhanced the HER activity (**Schemes 4F and 4G**). Recently, Qiao et al. prepared a V-Mo bimetallic nitridene solid solution V_{0.2}Mo_{0.8}N_{1.2} by catalytic molten-salt method (**Scheme 4H**).⁸⁹ The synthesis of molten-salt mean could reduce the growth energy barrier of V_{0.2}Mo_{0.8}N_{1.2}, which facilitated the V dissolution. It is theoretically showed that V doping results in the optimal electronic structure for rapid protons coupling to generate hydrogen (**Schemes 4I and 4J**). It is revealed that heteroatom doping in MXene could optimize the hydrogen adsorption energy, then increasing electrocatalyst activity of HER.

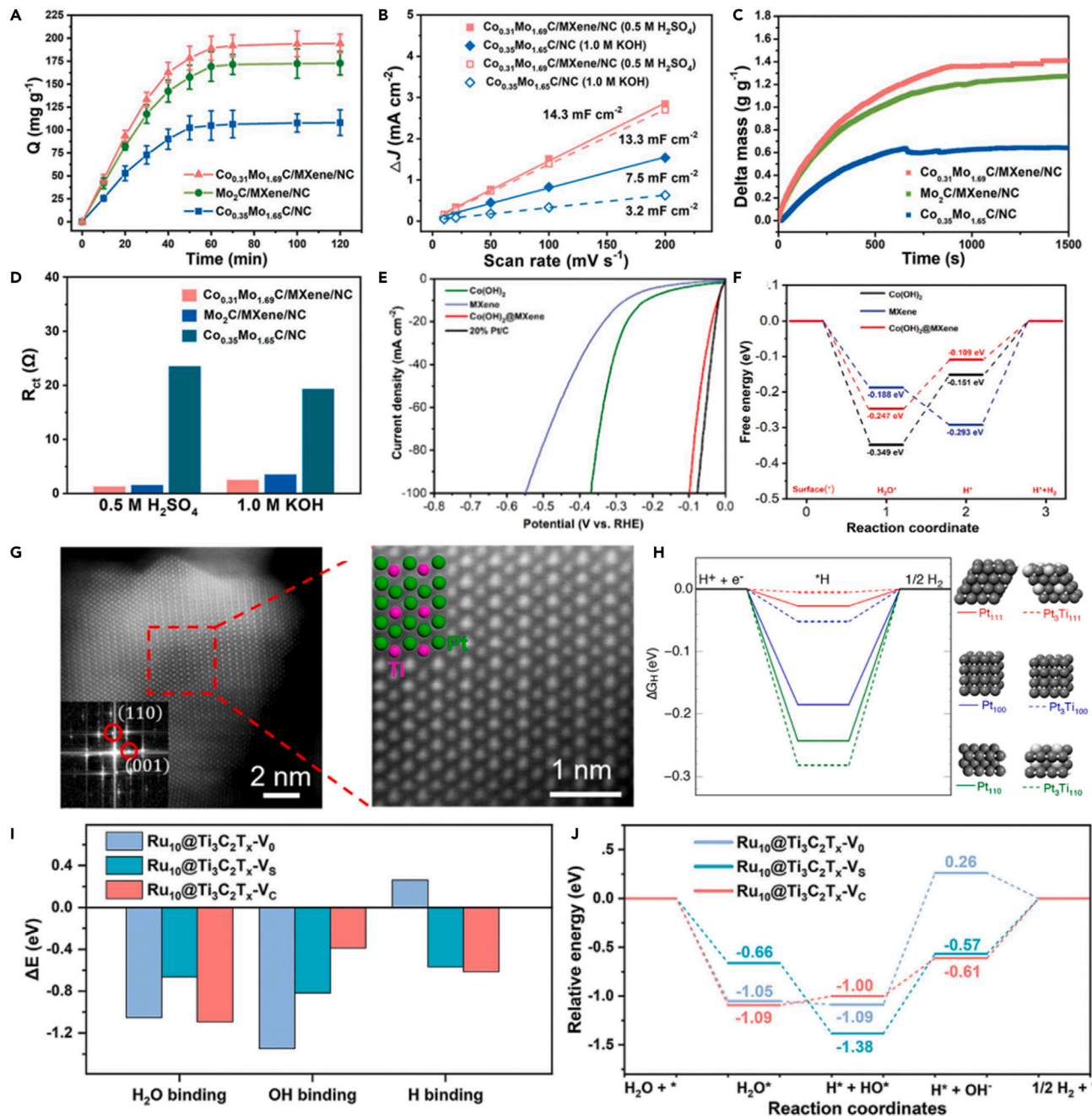
Thanks to the excellent hydrophilicity and electrical conductivity of MXenes, combining the MXene nanosheets with electrocatalytic active materials, such as transition metal compounds and noble metal species, can enhance the catalytic performance. Representative, Wang et al. developed a key strategy by engineering a multifunctional collaborative electrocatalytic interface among cobalt-molybdenum carbide, N-doped carbon, and Ti₃C₂T_x MXene (denoted as Co_xMo_{2-x}C/MXene/NC) to propel the HER in a wide pH and natural seawater.²³ In this case, the MXene could bring advantages of efficient H⁺/H₂O adsorption, large specific surface area, and low charge-transfer impedance, which accelerated the charge transfer kinetics of HER (**Schemes 5A–5D**). As another example, Peng et al. designed a new strategy of interfacial electron coupling by assembling transition-metal hydroxide with MXenes, including FeOOH@MXene, Co(OH)₂@MXene, and Ni(OH)₂@MXene, for alkaline HER.⁶² Consequently, Co(OH)₂@MXene showed outstanding catalytic activity for HER with a low overpotential of $\eta_j = 10 = 21.0$ mV, thanks to the favorable adsorption kinetics of water and hydrogen caused by the synergetic interfacial electron coupling effect between Co(OH)₂ and MXene (**Schemes 5E and 5F**). Also, this group reported the hybrid structure of CoC₂O₄ coated on MXene nanosheets for alkaline HER with a low overpotential of 28 and 216 mV at 10 and 1000 mA cm⁻².⁹⁰ The loading of active substances on the surface of MXene may also form a new highly active phase. In addition, *in situ* formation of Pt₃Ti NPs on Ti₃C₂T_x MXenes as catalysts for HER has been reported, in which the Pt underwent a temperature-dependent transition from single atoms into intermetallic compounds (**Scheme 5G**).⁶³ When the catalyst reduced at 550°C, the Pt/Ti₃C₂T_x-550 electrocatalyst outperformed commercial Pt/Vulcan and offered a low overpotential of $\eta_j = 10 = 32.7$ mV. It was suggested that the (111) and (100) surfaces of Pt₃Ti NPs exhibited more suitable hydrogen adsorption energy comparable to Pt (111) (**Scheme 5H**). In addition, Han et al. produced Ti vacancy cluster (Ti₃C₂T_x-V_C)-engineered MXenes through a facile HF etching method. The Ti vacancy clusters in Ti₃C₂T_x-V_C create unique lattice carbon ligand environment toward Ru species, which induces metal-support interaction.⁹¹ As a result, compared with nearly vacancy-free (Ti₃C₂T_x-V₀) and single Ti atom vacancy (Ti₃C₂T_x-V₅)-engineered MXenes, the Ti₃C₂T_x-V_C-modulated Ru clusters (Ru₁₀@Ti₃C₂T_x-V_C) exhibit superior electrocatalytic performance in the alkaline HER, due to the optimized balance of H₂O adsorption/dissociation and OH/H desorption (**Schemes 5I and 5J**).

What is more, MXenes can also serve as efficient carrier materials to host single-atom catalysts for HER, thanks to their abundant defect sites and adjustable structure. Typically, Zhang et al. reported double transition metal carbide Mo₂TiC₂T_x-MXene, with rich exposed base and Mo vacancy in the outer layer by electrochemical stripping.⁶⁴ The formed Mo vacancy was employed to fix single Pt atom to attain the catalyst of Mo₂TiC₂T_x-Pt_{SA}, thus greatly enhancing the catalytic activity for HER (**Scheme 6A**). The as-developed catalyst exhibited small overpotential of 30 and 77 mV at 10 and 100 mA cm⁻², respectively, and showed high mass activity about 40 times bigger than that of commercial 40% Pt/C (**Scheme 6B**). Further, it is calculated that the positively charged single Pt atoms loaded on MXene constitute the optimal adsorption position for H⁺, facilitating the HER (**Scheme 6C**). Also, Cui et al. developed the heterostructures of Pt-MXene-CNTs as HER catalysts.⁹² Significantly, nitrogen (N) and sulfur (S) co-doped Ti₃C₂T_x MXene have been reported to anchor ruthenium single atoms (Ru_{SA}) via N/S bonding (**Scheme 6D**). It is suggested that the Ru_{SA}-N-S-Ti₃C₂T_x electrocatalyst achieved an optimal ΔG_{H^+} of close to zero, enhancing the HER activity (**Scheme 6E**).⁶⁵ From the abovementioned, it is indicated that MXene is an effective single-atom carrier owing to its abundant defect sites and high surface activity. What is more, the exfoliated Ti₃C₂T_x-anchored Ru single atom was reported through a wet-chemistry impregnation.⁹³ The as-obtained Ru_{SA}@Ti₃C₂T_x showed excellent catalytic activity in alkaline HER, with a high current density of 1.5 A cm⁻² at 464.6 mV.

In another way, constructing 3D MXene structure can also promote the activity of HER electrocatalyst due to rich active sites and fast mass-charge transport channel.⁹⁴ As a typical example, 3D MXene structure with high conductivity, hydrophilicity, and chemical functionalization multilevel hollow structure, defined as mh-3D MXene, has been assembled by an effective template-engaged aerosol drying strategy (**Scheme 7A**). Coupling mh-3D MXene with Pt could create a high active catalytic interface, showing high stability, excellent H⁺/water



adsorption capacity, and fast charge-mass transport channel (Schemes 7B–7D).⁹⁵ Therefore, the mass activity of 2.4% Pt@mh-3D MXene was 10–20 times bigger than that of 20% Pt/C in acidic/alkaline solution, and the activity and durability were superior than 20% Pt/C in natural seawater (Schemes 7E and 7F). Similarly, Dang et al. reported a 3D self-supporting electrode by coconstructing the interfaces of Co_2P on MXene. As a result, the Co_2P grown on the surface of MXene ($\text{Ti}_3\text{C}_2\text{T}_x$)-modified Ni foam required a small overpotential of $\eta_{j=10} = 29$ mV



Scheme 5. MXene-based materials for HER

(A) Dependence of the amount of H^+ adsorbed on $\text{Co}_{0.31}\text{Mo}_{1.69}\text{C}/\text{MXene}/\text{NC}$, $\text{Mo}_2\text{C}/\text{MXene}/\text{NC}$ and $\text{Co}_{0.35}\text{Mo}_{1.65}\text{C}/\text{NC}$ catalysts on the adsorption time.

(B) The plots of current density differences (Δj) against scan rates at 0.25 V vs. RHE for $\text{Co}_{0.31}\text{Mo}_{1.69}\text{C}/\text{MXene}/\text{NC}$ and $\text{Co}_{0.35}\text{Mo}_{1.65}\text{C}/\text{NC}$ catalysts.

(C) Mass change as a function of time for water adsorption on $\text{Co}_{0.31}\text{Mo}_{1.69}\text{C}/\text{MXene}/\text{NC}$, $\text{Mo}_2\text{C}/\text{MXene}/\text{NC}$ and $\text{Co}_{0.35}\text{Mo}_{1.65}\text{C}/\text{NC}$ catalysts.

(D) A comparison in charge-transfer impedance for HER. Copyright 2019 WILEY-VCH Verlag GmbH & Co. KGaA, Weinheim.

(E) HER polarization curves of 20% Pt/C, Co(OH)_2 , MXene, and $\text{Co(OH)}_2@\text{MXene}$ catalysts.

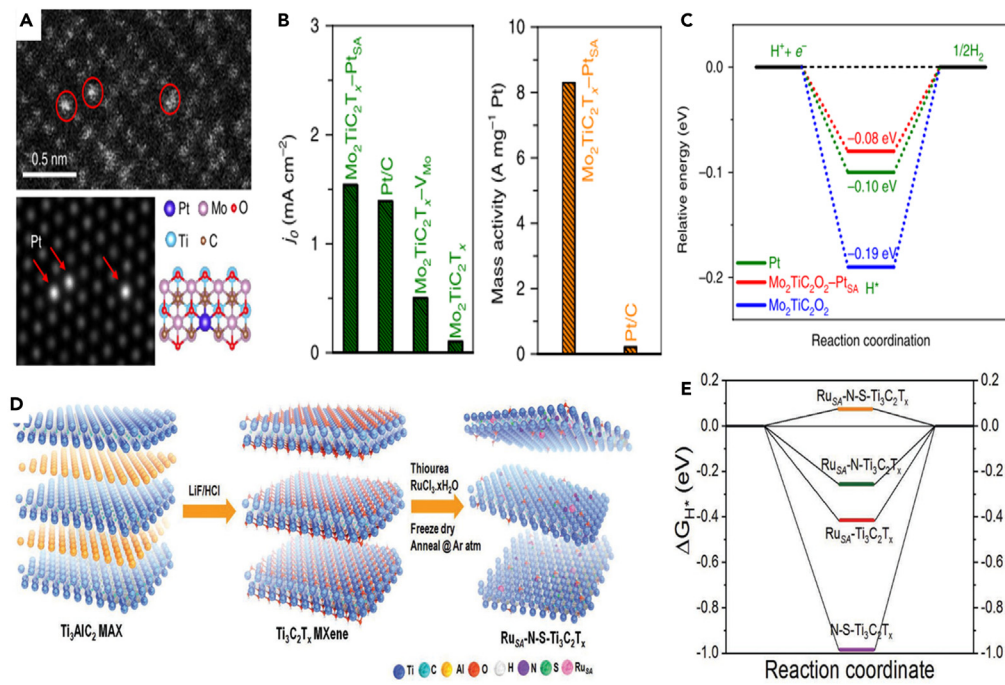
(F) Gibbs-free energy profiles of the alkaline HER at the equilibrium potential for Co(OH)_2 , MXene, and $\text{Co(OH)}_2@\text{MXene}$, respectively.⁶² Copyright the Royal Society of Chemistry 2021.

(G) Atomic-resolution HAADF-STEM image of $\text{Pt/Ti}_3\text{C}_2\text{T}_x$ -550.

(H) Simulated STEM image of Pt_3Ti along the [110] direction.⁶³ Copyright 2019 American Chemical Society.

(I) The binding energy of H_2O , OH, and H on $\text{Ru}_{10}@\text{Ti}_3\text{C}_2\text{T}_x$ models.⁹¹ Copyright 2023 Wiley-VCH GmbH.

(J) Relative energy diagram during HER for $\text{Ru}_{10}@\text{Ti}_3\text{C}_2\text{T}_x$ models.⁹¹ Copyright 2023 Wiley-VCH GmbH.



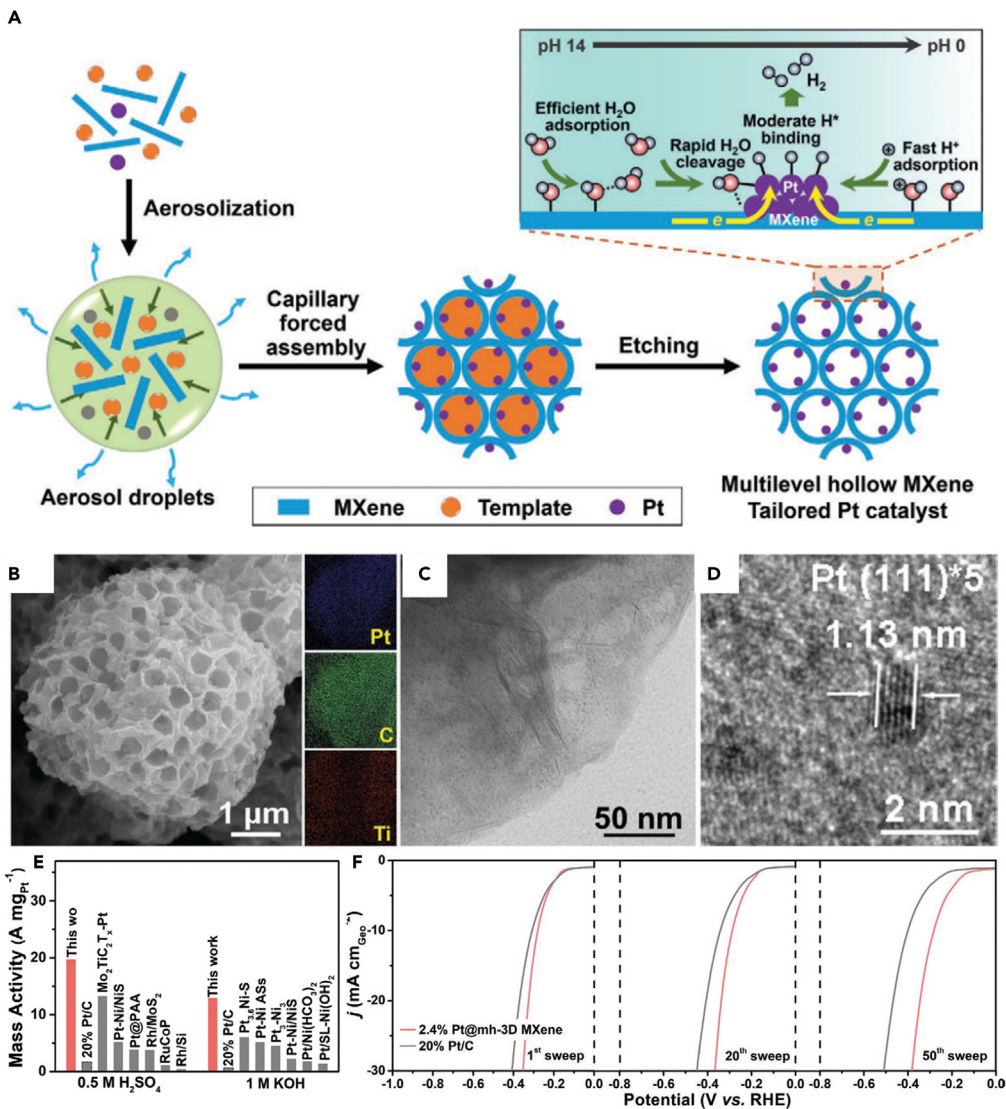
Scheme 6. MXene anchoring single-atom catalyst for HER

- (A) Magnified HAADF-STEM image of $\text{Mo}_2\text{TiC}_2\text{T}_x\text{-Pt}_{\text{SA}}$ and its corresponding simulated image and illustration of the structure of $\text{Mo}_2\text{TiC}_2\text{T}_x\text{-Pt}_{\text{SA}}$.
- (B) Exchange current densities of the catalysts and the mass activity of state-of-the-art Pt/C and $\text{Mo}_2\text{TiC}_2\text{T}_x\text{-Pt}_{\text{SA}}$.
- (C) Calculated free energy profiles of HER at the equilibrium potential for $\text{Mo}_2\text{C}_2\text{O}_2$, $\text{Mo}_2\text{TiC}_2\text{T}_x\text{-Pt}_{\text{SA}}$, and Pt/C.⁶⁴ Copyright 2018 Springer Nature.
- (D) Synthesis and morphological characterizations of $\text{Ru}_{\text{SA}}\text{-N-S-Ti}_3\text{C}_2\text{T}_x$ catalyst.
- (E) The calculated Gibbs hydrogen adsorption free energy ($\Delta G_{\text{H}*}$) diagram.⁶⁵ Copyright 2019 WILEY-VCH Verlag GmbH & Co. KGaA, Weinheim.

for HER in 1.0 M KOH.⁵² Moreover, Yu et al. coupled La-doped NiFe-LDH on 3D vertically aligned $\text{Ti}_3\text{C}_2\text{T}_x$ MXene onto NF skeleton (named as NiFeLa-LDH/v-MXene/NF) for water splitting, which showed higher activity than NiFeLa-LDH/NF without MXene and commercial Pt/C/NF catalyst.⁵³ It is shown that 3D MXene structure could promote HER activity, due to the larger reactive surface area, sufficient meso-/macro-porous channels for mass-charge transport, and 3D continuous fast conductive channel.

The stability of the catalyst is also an important factor that should be considered in the application of electrocatalysis. Therefore, some key strategies were proposed to inhibit the oxidation of MXenes, maintain excellent physical and chemical properties, and thus improve the durability of the catalyst.⁷⁷ In order to restrain the problem that MXenes can be oxidized in the hydrothermal process at high temperature, carbon coating on the surface of MXene has been proved to be an effective strategy to inhibit the oxidation of MXene, even in high-temperature hydrothermal environment (Scheme 8A).²² Consequently, the $\text{MoS}_2/\text{Ti}_3\text{C}_2@\text{C}$ electrocatalyst exhibited an overpotential of $\eta_{j=10} = 135$ mV, which was better than that of MoS_2 /oxidized MXene catalysts due to the well-maintained structure and properties of MXene, such as 2D structural feature, excellent conductivity, and high surface activity (Schemes 8B and 8C).²² *In situ* conversion of MXene surface to stable active phase could also inhibit the oxidation of MXene effectively. The oxidation of Mo_2CT_x were avoided by *in situ* sulfidation to form a $\text{Mo}_2\text{CT}_x/2\text{H}-\text{MoS}_2$ hybrid structure (Scheme 8D). This method not only inhibited the oxidation of MXene but also formed the strong interaction between Mo_2CT_x and 2H-MoS₂ within the nanohybrid structure, accelerated electron transport, in comparison with the physiosorbed nanohybrid. As a result, the $\text{Mo}_2\text{CT}_x/2\text{H}-\text{MoS}_2$ nanohybrid could achieve industrially current density of over $-450 \text{ mA cm}^{-2}_{\text{geom}}$ with outstanding durability. Notably, the $\text{Mo}_2\text{CT}_x/2\text{H}-\text{MoS}_2$ nanohybrid could work stably for 10 days with a less than 30 mV overpotential increase (Schemes 8E and 8F).⁷⁷ It is validated that reducing the surface-oxygen-containing functional groups and *in situ* transformation of MXene into high catalytic activity and stability substances can inhibit the oxidation of MXene, thus increasing the stability and expanding the applications of catalysts.

As a result, MXenes present many promising applications in HER, thanks to the excellent physical and chemical properties of MXene that meet the needs of HER catalysts. For example, the excellent electrical conductivity ensures the rapid transport of electrons. And the high hydrophilicity promotes the adsorption of water, which is the initial reactant of HER in neutral/alkaline environment. The following strategies have been considered to improve the activity and stability of MXene-based electrocatalysts for HER. (1) Heteroatomic doping of MXene can tune the electronic structure of active center to boost its catalytic performance. (2) The high surface activity and abundant defect sites of MXenes allow them to be coupled with active materials, including single-atom catalysts, nanoparticles, and 2D nanosheet, which can construct high-activity synergistic catalytic interface. (3) Constructing 3D MXene framework can offer more active sites, as well as charge/mass transport channels, avoiding the stacking of 2D nanosheets. And (4) covering the surface of MXene or *in situ* converting the surface of MXene to active material can avoid the oxidation of MXene and thus enhance the durability of electrocatalyst. Although many strategies have been developed to greatly

**Scheme 7. 3D MXene-based catalyst for HER**

(A) Schematic illustration of template-engaged ultrafast aerosol drying strategy for yielding multilevel hollow MXene tailored low-Pt catalyst with multifunctional catalytic interface and its benefit in promoting the HER under multi-pH conditions.

(B) SEM image and elemental mapping analysis of Pt@mh-3D MXene.

(C) TEM image of Pt@mh-3D MXene.

(D) HRTEM image of Pt nanocrystallites on mh-3D MXene.

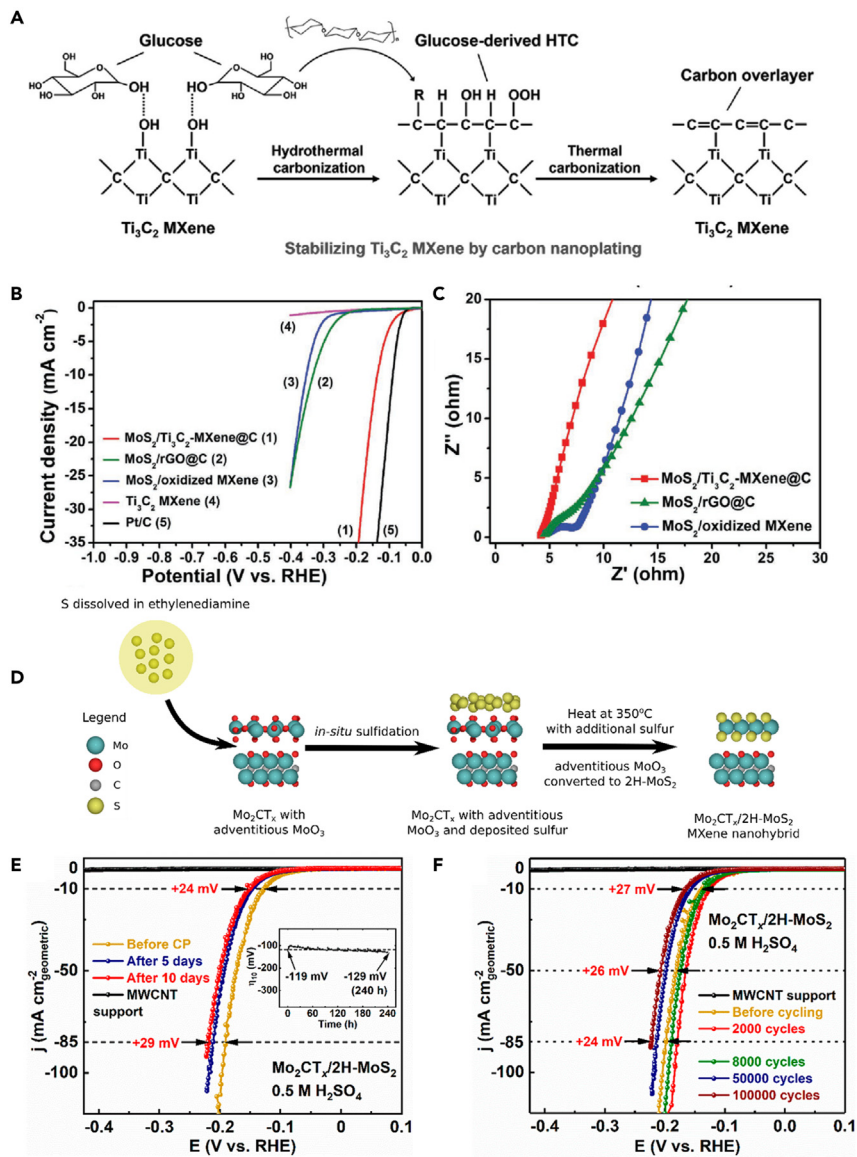
(E) A comparison between 2.4% Pt@mh-3D MXene and reported noble metal catalysts in mass activity at $\eta = 100$ mV.

(F) Polarization curves of 2.4% Pt@mh-3D MXene and 20% Pt/C for 1st, 20th, and 50th sweeps in natural seawater.⁹⁵ Copyright 2020 WILEY-VCH Verlag GmbH & Co. KGaA, Weinheim.

boost the HER performance of MXene-based electrocatalysts, the activity and stability of these current catalysts reported are still difficult to meet the needs of industrial production. The electrocatalysts with high current density ($>1000 \text{ mA cm}^{-2}$) and long life ($>1000 \text{ h}$) can be obtained by developing new MXene with high intrinsic catalytic activity and stability and accelerating the mass transfer process of the catalyst.

MXene-based materials for carbon dioxide reduction reaction

The electrochemical CO₂RR is a promising technology to reduce CO₂ emissions and obtain high-valued chemicals with a sustainable and economical strategy.³ In this regard, MXene-based materials also show outstanding performance on CO₂RR.⁹⁶ For instance, Yang et al. developed a single-atom copper loaded on MXene layers by selective etching of Al layers from quaternary MAX phases [Ti₃(Al_{1-x}Cu_x)C₂], due to the easy sublimation properties of AlCl₃, remaining the unreacted Cu element on the MXene (Schemes 9A and 9B).³ As a result, the



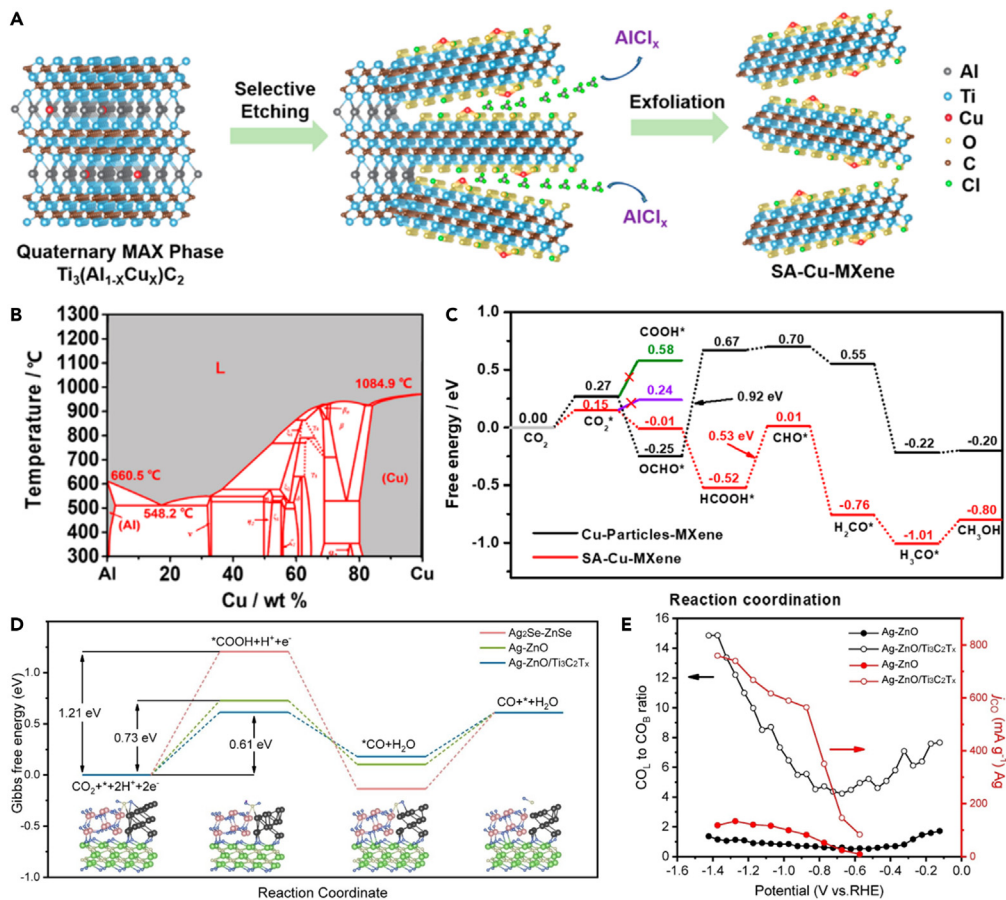
Scheme 8. Stabilizing MXene-based catalyst for HER

(A) Schematic illustration of the strategy for stabilizing Ti₃C₂ MXene by carbon nanoplating.

(B) Polarization curves and (C) electrochemical impedance spectroscopy of MoS₂/Ti₃C₂@C and MoS₂/oxidized MXene.²² Copyright 2017 WILEY-VCH Verlag GmbH & Co. KGaA, Weinheim.

(D) In situ sulfidation of d-Mo₂CT_x to produce Mo₂CT_x/2H-MoS₂ nanohybrid. IR-corrected CV polarization curves for Mo₂CT_x/2H-MoS₂ nanohybrid in 0.5 M H₂SO₄ after (E) 10 days constant current test and (F) 100,000 accelerated CV cycling at 100 mV s⁻¹.⁷⁷ Copyright 2020 American Chemical Society.

single-atom-Cu-MXene electrocatalyst exhibited a high Faradic efficiency (FE) of 59.1% to produce CH₃OH with high stability, delivering a low energy barrier of rate-determining step (HCOOH* converted to CHO*) (Scheme 9C). It was shown that the multi-elements with the alloying feature could randomly took up the single-atom thick A layers in MAX phase, making MAX an ideal platform to produce single-atom catalyst. Meanwhile, Pan et al. predicted the high catalytic activities of single-atom Sc, Ti, and V supported Ti₂CN₂ to produce CO. Particularly, single-atom Mn and Fe on Ti₂CN₂ were predicted to be active center for the production of HCOOH.⁹⁷ In addition, MXene can also regulate the electronic structure of active center to promote the electrochemical CO₂ reduction performance of electrocatalyst. For instance, the Ag-ZnO/Ti₃C₂T_x electrocatalyst achieves an outstanding CO₂ conversion performance of a nearly 100% CO Faraday efficiency with a high current density of 22.59 mA cm⁻² at -0.87 V vs. RHE, which is attributed to the optimized electronic structure of MXene-regulated Ag-ZnO interfaces having a low intermediate formation energy barrier (Scheme 9D).⁹⁸ In situ ATR-IR spectra reveal that the dominated linear-bonded CO (CO_l) intermediate had an accelerated CO desorption rate on Ag-ZnO/Ti₃C₂T_x (Scheme 9E), which was highly correlated with the partial current of CO formation. What is more, Maryam et al. reported 3D Cu-Pd/MXene aerogels for

**Scheme 9. MXene-based catalyst for CO₂RR**(A) Schematic illustration of the fabrication of SA-Cu-MXene via selective etching quaternary MAX- $\text{Ti}_3(\text{Al}_{1-x}\text{Cu}_x)\text{C}_2$.

(B) Al–Cu binary phase diagram.

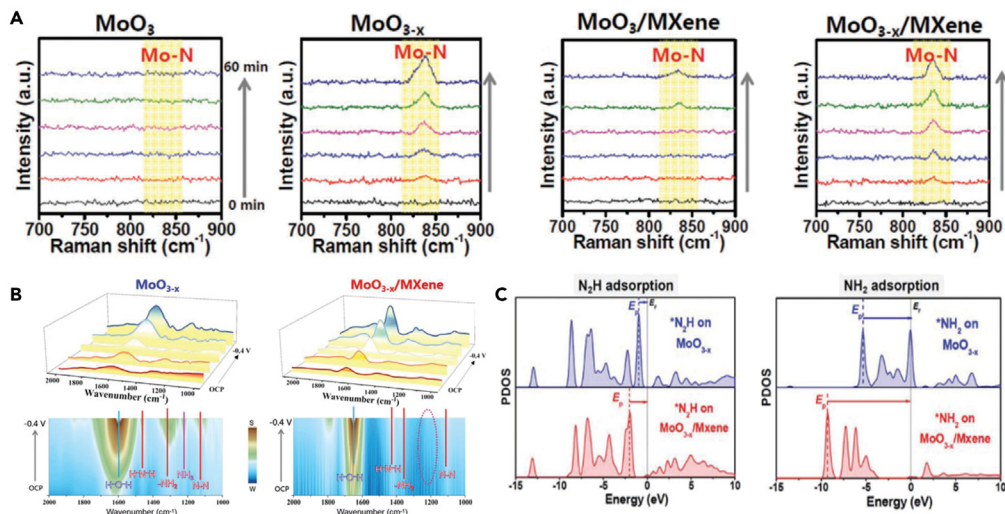
(C) Free energy diagram of CO₂ to CH₃OH on Cu-O₃ structure.³ Copyright 2021 American Chemical Society.(D) The free energy diagrams of electrochemical CO₂ reduction.(E) CO_L to bridge-bonded CO (CO_B) band intensity ratio and mass-specific activity of Ag-ZnO and Ag-ZnO/Ti₃C₂T_x derived from the ATR-IR spectra.⁹⁸ Copyright 2023 Wiley-VCH GmbH.

CO₂RR, with formate selectivity >90%,⁹⁹ whereas Cu-Pd aerogel achieved near-unity CO production without the MXene templating. These results show that MXene can not only promote reaction rate but also change the reaction pathway.

The surface functional groups of MXene also affect the catalytic performance and selectivity of CO₂RR. Replacing the O-terminations with F-terminations on Ti₂CT_x altered the *COOH adsorption energy, thus a smaller overpotential could be found at lower amounts of -F termination.¹⁰⁰ And Handoko et al. reported that on most O-terminated MXenes, the CO₂ reduction pathway to CH₄ prefers the formation of the *HCOOH intermediate as opposed to the *CO intermediate.¹⁰¹

MXene-based materials for nitrogen reduction reaction

The reduction of nitrogen can produce platform chemical ammonia NH₃, which is widely applied in the industry and agriculture, in a sustainable and environmental manner, and help the global nitrogen cycle.¹⁰² As reported previously, MXenes can not only be used as platform material for NRR but also can accelerate NRR process. For example, Chu et al. demonstrated the O-vacancy-rich MoO_{3-x} attached on Ti₃C₂T_x-MXene (MoO_{3-x}/MXene) for NRR, exhibiting outstanding activity for NRR with NH₃ yield of 95.8 μg h⁻¹ mg⁻¹ and an FE of 22.3%. In situ Raman spectra showed that the MoO_{3-x} served as the catalytic center for N₂ adsorption and activation (Scheme 10A).¹⁰³ In situ Fourier transform infrared spectroscopy (FTIR) suggested that the produced NH₃ was easy desorption from the MoO_{3-x}/MXene surface, facilitating re-exposure of the active sites (Scheme 10B). It was revealed from density functional theory calculation that MXene could further modulate the O-vacancy sites and effectively stabilize *N₂/*N₂H, while destroying the stability of *NH₂/*NH₃, thus optimizing the binding energy of NRR intermediates, reducing energy barriers, and enhancing the catalytic activity of MoO_{3-x}/MXene for NRR (Scheme 10C). This work reflected the promoting effect of MXenes for NRR. Further, Hui et al. computational screened single-atom catalysts (i.e., Y, Zr, Nb, Hf, Ta, W, Re, and Os) on



Scheme 10. MXene-based catalyst for NRR

- (A) *In situ* Raman spectroscopy investigations of various catalysts.
 (B) *In situ* FTIR spectra (top) and corresponding contour maps (bottom) of MoO_{3-x} and MoO_{3-x}/MXene at various potentials.
 (C) PDOS of *N₂H and *NH₂ intermediates on MoO₃/MXene and MoO_{3-x}/MXene.¹⁰³ Copyright 2021 Wiley-VCH GmbH.

the Mo vacancies of MoCO₂ MXene (Mo₂CO₂-M_{SA}) for NRR.^{102,104} Among them, Mo₂CO₂-Y_{SA} showed the lowest reaction energy barrier of 0.08 eV with high selectivity for NRR. In addition, the formation energy of Mo₂CO₂-Y_{SA} was lower, exhibiting higher feasibility for experimental synthesis of the Mo₂CO₂-Y_{SA} catalyst.

MXene-based materials for other catalytic reactions

Recently, the application of MXene in electrocatalysis has been further extended. For example, MXene-based electrocatalysts can be developed for hydrazine oxidation reaction (HzOR). For example, Ti₃C₂T_x-MXene has been reported to support Ni single-atom catalysts (Ni SACs/Ti₃C₂T_x) by the assistance of rich Ti vacancies.¹⁰⁵ As a result, the Ni SACs/Ti₃C₂T_x showed an ultralow onset potential (-0.03 V vs. RHE) for HzOR. It is calculated that surrounding C atoms can optimize the electronic density of states of Ni single atoms, improving the electrocatalytic activity of Ni SACs/Ti₃C₂T_x. What is more, NiCo@C/MXene/Cu foam required ultralow potentials of -25 and 43 mV to achieve high current densities of 100 and 500 mA cm⁻², respectively, for HzOR.¹⁰⁶

In addition, MXene-based materials can be applied for nitrate reduction reaction (NO₃RR) to produce NH₃ and achieve the global nitrogen cycle. The Fe-substituted Mo-based MXene (Mo₂CT_x:Fe) outperformed excellent activity for NO₃RR with FE and NH₃ yield rate of 41% and $3.2\text{ }\mu\text{mol h}^{-1}\text{ mg}^{-1}$ in acidic media and 70% and $12.9\text{ }\mu\text{mol h}^{-1}\text{ mg}^{-1}$ in neutral media, respectively.¹⁰⁷ The Fe promotes the formation of O vacancy, resulting in high activity of NO₃RR. Besides, Fe single atom has anchored on Ti₃C₂T_x MXene (FeSA/Mxene) for NO₃RR with high NH₃ FE and selectivity of 82.9% and 99.2%, respectively.¹⁰⁸ Moreover, MXene-based materials were also used for other electrocatalytic reactions. For instance, CoS₂ nanoparticles with similar size in carbon matrix on MXene-wrapped NF showed excellent electrocatalytic activity for sulfion oxidation reaction (S²⁻–2e⁻ = S).¹⁰⁹ The O-terminated MXene (Ti₃C₂O₂) has been reported for perfluorooctanoic acid oxidation with an oxidation rate constant of $3.9 \times 10^{-2}\text{ min}^{-1}$.¹¹⁰

CONCLUSIONS AND PERSPECTIVE

The attractive properties of MXenes such as metallic conductivity, hydrophilic nature, and large specific surface area enable it to be a promising class of 2D materials for constructing multifunctional high-performance electrocatalysts with high activity and stability. However, bare MXenes are difficult to meet the needs of practical applications for electrocatalyst, due to easy restacking, poor antioxidant capacity, and limited intrinsic catalytic activity. In this review, many key strategies have been developed to solve these issues, such as (1) introducing the interlayer spacers including CNT, including 0D NPs, 1D nanotubes/nanowires, and 2D nanosheets, (2) processing MXenes into hierarchical 3D architecture by ultrasonic-assisted aerosol spray drying, template method, and preparation of aerogel, (3) heteroatomic doping with metal or nonmetal, (4) surface-modifying MXenes with high active materials including metal ion, transition metal oxides, transition metal dichalcogenides, or transition metal carbide, (5) *in situ* conversion of MXene surfaces to oxide or sulfide, and (6) covering the edge of MXenes with other molecules, including carbon nanolayer, ion, or organic polymer to prevent oxidation.

As a result, thanks to these promising strategies, MXene-based materials have shown excellent catalytic activity and long durability for ORR, OER, HER, CO₂RR, and NRR. And the MXene-based materials for HER, OER, and CO₂RR have been summarized in Table 1. The possible key reasons are summarized in the following: (1) reducing the restacking of MXenes can provide larger specific surface area, high porosity, and short ion and mass transport distance, so that electrochemically active sites are easily accessed to facilitate the sufficient electrocatalytic reactions.

Table 1. Summary of the reported MXene-based materials for electrocatalysis

Catalyst	Electrolyte	Reaction	Potential (V vs. RHE)	Reference
Mo ₂ CT _x /2H-MoS ₂	0.5 M H ₂ SO ₄	HER	-0.119 (<i>j</i> = 10) -0.182 (<i>j</i> = 100)	Lim et al. ⁷⁷
Pt-MXene-single-walled carbon nanotubes	0.5 M H ₂ SO ₄	HER	-0.062 (<i>j</i> = 10)	Cui et al. ⁹²
P-doped V ₂ CT _x	0.5 M H ₂ SO ₄	HER	-0.163 (<i>j</i> = 10)	Yoon et al. ⁵⁴
Ru _{SA} -N-S-Ti ₃ C ₂ T _x	0.5 M H ₂ SO ₄	HER	-0.076 (<i>j</i> = 10)	Ramalingam et al. ⁶⁵
MoS ₂ /Ti ₃ C ₂ -MXene@C	0.5 M H ₂ SO ₄	HER	-0.135 (<i>j</i> = 10)	Wu et al. ²²
V _{0.2} M _{0.8} N _{1.2}	0.5 M H ₂ SO ₄	HER	-0.158 (<i>j</i> = 10)	Jin et al. ⁸⁹
Mo ₂ TiC ₂ T _x -Pt _{SA}	0.5 M H ₂ SO ₄	HER	-0.030 (<i>j</i> = 10) -0.077 (<i>j</i> = 100)	Zhang et al. ⁶⁴
Mo ₂ CT _x -Co	1.0 M H ₂ SO ₄	HER	-0.18 (<i>j</i> = 10)	Kuznetsov et al. ⁵⁷
Pt/Ti ₃ C ₂ T _x	0.1 M HClO ₄	HER	-0.032 (<i>j</i> = 10)	Li et al. ⁶³
Ru@Ti ₃ C ₂ T _x -V _c	1.0 M KOH	HER	-0.035 (<i>j</i> = 10) -0.463 (<i>j</i> = 1000) -0.488 (<i>j</i> = 1500)	Wang et al. ⁹¹
Co _{0.31} Mo _{1.69} C/MXene/NC	1.0 M KOH 0.5 M H ₂ SO ₄	HER	-0.075 (<i>j</i> = 10) -0.081 (<i>j</i> = 10)	Wu et al. ²³
NiCo@Nb-doped Ti ₃ C ₂ T _x MXene	1.0 M KOH	HER	-0.043 (<i>j</i> = 10)	Du et al. ⁵⁵
Co ₂ P/N@Ti ₃ C ₂ T _x @NF	1.0 M KOH	HER	-0.015 (<i>j</i> = 10)	Lv et al. ⁵²
2.4% Pt@multilevel hollow-3D MXene	1.0 M KOH 0.5 M H ₂ SO ₄	HER	-0.027 (<i>j</i> = 10) -0.013 (<i>j</i> = 10)	Xiu et al. ⁹⁵
Ru _{SA} @Ti ₃ C ₂ T _x	1.0 M KOH	HER	-0.425 (<i>j</i> = 1000) -0.464 (<i>j</i> = 1500)	Zou et al. ⁹³
Co(OH) ₂ @MXene	1.0 M KOH	HER	-0.021 (<i>j</i> = 10)	Li et al. ⁶²
CoC ₂ O ₄ @MXene	1.0 M KOH	HER	-0.028 (<i>j</i> = 10) -0.216 (<i>j</i> = 1000)	Wang et al. ⁹⁰
NiFeLa-LDH/vertically-MXene/NF	1.0 M KOH	HER OER	-0.233 (<i>j</i> = 500) 1.485 (<i>j</i> = 500)	Yu et al. ⁵³
CoP@3D Ti ₃ C ₂ -MXene	1.0 M KOH	OER	1.618 (<i>j</i> = 10)	Xiu et al. ³⁸
Ti ₃ C ₂ T _x -CoBDC	1.0 M KOH	OER	1.64 (<i>j</i> = 10)	Zhao et al. ⁶¹
Co/N-CNTs@ Ti ₃ C ₂ T _x	0.1 M KOH	OER	1.641 (<i>j</i> = 10)	Zhang et al. ⁸⁶
Overlapped g-C ₃ N ₄ and Ti ₃ C ₂ nanosheets	0.1 M KOH	OER	1.65 (<i>j</i> = 10)	Ma et al. ⁶⁰
SA-Cu-MXene	0.1 M KHCO ₃	CO ₂ RR to methanol	-1.4 (<i>j</i> = 21.3)	Zhao et al. ³
Cu-Pd-MXene	0.1 M KHCO ₃	CO ₂ RR to formate	-0.9 (<i>j</i> = 16.2)	Abdinejad et al. ⁹⁹
Ag-ZnO/Ti ₃ C ₂ T _x	0.5 M KHCO ₃	CO ₂ RR to CO	-0.87 (<i>j</i> = 22.59)	Hao et al. ⁹⁸

(2) Surface-modifying or *in situ* conversion MXenes with high active materials can maintain the advantages of MXenes, such as high electrical conductivity and hydrophilicity, short ion transport distance, and enhance the activity of the electrocatalysts by providing more active sites, further optimizing the electronic structure of the active centers, and preventing the aggregation of active materials. (3) Heteroatomic doping can optimize the electronic structure of MXenes that provide new active sites for electrocatalytic reaction. And (4) inhibiting the oxidation of MXenes can maintain the excellent electrical conductivity, improve the stability, and broaden the application range of MXenes to high-temperature reactions.

Despite the significant progress made, we are still facing several key challenges of MXene-based electrocatalysts used in actual industrial production. The following high-priority research directions should be considered fully.

Low-cost mass production of MXene

To expand the practical application of MXenes, it is urgently necessary to develop new MXene production methods with large scale and low cost at mild conditions. The commonly used HF and fluoride salt etching methods are highly toxic and low yield, which limits the large-scale preparation of MXenes. Notably, Hao et al. developed a very promising strategy based on thermal-assisted electrochemical etching to synthesize MXenes (e.g., Ti₂CT_x, Cr₂CT_x, and V₂CT_x).¹¹¹ Further, more types of MXenes should be investigated using this method. The molten salt etching method is also efficient for producing high-quality 2D MXenes without using toxic reagents.^{112,113} However, the stripping, surface

modification, and defect site construction of MXenes etched by molten salt method still need to be studied. In addition, Yang et al. proposed a supercritical etching method for large-scale and rapid production of MXenes assisted by supercritical carbon dioxide.¹¹⁴ As a result, five typical MXenes ($Ti_3C_2T_x$, Nb_2CT_x , Ti_2CT_x , Mo_2CT_x , and Ti_3CNT_x) can be prepared with the yield of ~ 1 kg. Researchers are constantly exploring new low-cost, large-scale preparation methods for MXenes, but there is still a long way to go.

Synthesis of MXene with high catalytic activity

Recently, high-entropy materials exhibit excellent electrocatalytic activity due to their abundant composition and multiple and tunable active sites.^{115,116} Some high-entropy transition-metal carbide (HE-MXene) have been synthesized, such as $(Ti_{1/5}V_{1/5}Zr_{1/5}Nb_{1/5}Ta_{1/5})_2AlC$,¹¹⁷ $TiVNbMoC_3T_x$, and $TiVCrMoC_3T_x$.¹¹⁸ HE-MXene performs well in energy storage; however, HE-MXene is rarely used in electrocatalysis so far. DFT calculation was used to compare the reaction energy barrier of HER between HE-MXene $TiVNbMoC_3$ and V_4C_3 , both with the O terminations. It is indicated that the HE-MXene displayed optimal H adsorption, which was much closer to zero (-0.41 eV) compared with $V_4C_3O_2$ (-0.97 eV), showing more favorable reaction energy barrier when using the HE-MXene. Therefore, it is promising to develop many kinds of HE-MXene for different electrocatalytic reactions. In another way, a new MXene material, boridene, had been reported recently.¹⁶ It is predicted that 2D metal borides (MBenes), Mo_2B_2 , Ti_2B_2 , and Cr_2B_2 , could be used for electrocatalytic coupling of N_2 and CO_2 to produce urea by DFT computations.¹¹⁹ Meanwhile, Sun et al. predicted that Mo_2B_2 -MBene-supported single-atom catalysts (Ti , V , Cr , Mn , Fe , Co , Ni , and Cu) could be used for HER, OER, and ORR.¹²⁰ However, the stable, large-scale production of MBene still needs to be explored to expand its application in electrocatalysis. In addition, fluorine-free synthesized Ta_2C MXene displayed excellent catalytic activity for HER and nitrophenol reduction.¹²¹

High-current and long-life MXene-based electrocatalyst

To satisfy the need of industrial production, catalysts are highly needed to offer a high current density of >500 mA cm $^{-2}$ and long-life performance of >1000 h. For water splitting, the catalysts with high current density and long life need a fast charge and mass transport channels, excellent hydrophilicity and gas-phobicity, high intrinsic catalytic activity, and structural stability.¹²² MXene-based materials are of great application potential that the current density of reconfiguration- $CoC_2O_4@MXene$ and $Ru_{SA}@Ti_3C_2T_x$ catalyst could reach up to 1,300 and 1,600 mA cm $^{-2}$ for HER, respectively.⁹⁰ In addition, the current density is affected by the electron transport process, especially the electron transport at the interface between the catalyst and the support.¹⁰⁰ Thus, the surface of highly conductive MXene can be *in situ* converted to produce highly active substances. The close link between catalyst and support can effectively reduce the interface resistance. On the other hand, for catalytic reaction with large density current, the mass transfer between gas-liquid-solid is also a decisive factor. The NiCo-MOF on MXene-wrapped Cu foam ($NiCo@C/MXene/CF$) electrocatalyst has been reported to have larger bubble contact angle of 153° than the $NiCo@C/CF$ electrocatalyst without MXene in seawater for HER, resulting in faster release of smaller gas bubbles, which promoted interfacial stability and facilitates continued exposure of catalytic sites at large current density.¹⁰⁶ These results show the potential of MXene for electrocatalysis in large current density. However, the life of MXene in electrocatalysis still needs to be improved. DFT calculation results show that MXene will be poisoned at specific pH and voltage.⁸⁷ Therefore, characterizing the reconstruction of MXene during electrocatalysis and determining the real active site are helpful to enhance the stability of MXene-based materials. Nevertheless, MXene-based electrocatalysts with high current density and long life should be continually developed. To achieve this goal, the electrocatalysts need to have enough active sites and are conducive to the adsorption of reactants and desorption of products.

In short, we believe that this review will offer close insight to develop highly active and durable MXene-based electrocatalysts and open many promising opportunities for practical application of MXene-based electrocatalysts in the near future.

ACKNOWLEDGMENTS

This work was financially supported by the National Natural Science Foundation of China (Grants 22125903, 22209174), Dalian Innovation Support Plan for High Level Talents (2019RT09), Dalian National Laboratory for Clean Energy For Clean Energy (DNL), CAS, DNL Cooperation Fund, CAS (DNL202016, DNL202019), and China Postdoctoral Science Foundation (2021M703143).

AUTHOR CONTRIBUTIONS

Z.-S.W. proposed and supervised the overall project. X.-H.W., Y.W., and Z.-S.W. wrote the manuscript.

DECLARATION OF INTERESTS

The authors declare no competing interests.

REFERENCES

1. Seh, Z.W., Kibsgaard, J., Dickens, C.F., Chorkendorff, I., Nørskov, J.K., and Jaramillo, T.F. (2017). Combining theory and experiment in electrocatalysis: Insights into materials design. *Science* 355, eaad4998.
2. Wang, J., Xu, F., Jin, H., Chen, Y., and Wang, Y. (2017). Non-noble metal-based carbon composites in hydrogen evolution reaction: fundamentals to applications. *Adv. Mater.* 29, 1605838.
3. Zhao, Q., Zhang, C., Hu, R., Du, Z., Gu, J., Cui, Y., Chen, X., Xu, W., Cheng, Z., Li, S., et al. (2021). Selective etching quaternary MAX phase toward single atom copper immobilized MXene ($Ti_3C_2Cl_x$) for efficient

- CO_2 electroreduction to methanol. *ACS Nano* 15, 4927–4936.
4. Liu, Y., Liu, X., Lv, Z., Liu, R., Li, L., Wang, J., Yang, W., Jiang, X., Feng, X., and Wang, B. (2022). Tuning the spin state of the iron center by bridge-bonded Fe-O-Ti ligands for enhanced oxygen reduction. *Angew. Chem. Int. Ed.* 61, e202117617.
 5. Tsounis, C., Kumar, P.V., Masood, H., Kulkarni, R.P., Gautam, G.S., Müller, C.R., Amal, R., and Kuznetsov, D.A. (2023). Advancing MXene electrocatalysts for energy conversion reactions: surface, stoichiometry, and stability. *Angew. Chem. Int. Ed.* 62, e202210828.
 6. Zhao, X., Xu, H., Hui, Z., Sun, Y., Yu, C., Xue, J., Zhou, R., Wang, L., Dai, H., Zhao, Y., et al. (2019). Electrostatically assembling 2D nanosheets of MXene and MOF-derivatives into 3D hollow frameworks for enhanced lithium storage. *Small* 15, 1904255.
 7. Naguib, M., Kurtoglu, M., Presser, V., Lu, J., Niu, J., Heon, M., Hultman, L., Gogotsi, Y., and Barsoum, M.W. (2011). Two-dimensional nanocrystals produced by exfoliation of Ti_3AlC_2 . *Adv. Mater.* 23, 4248–4253.
 8. Bai, X., and Guan, J. (2022). MXenes for electrocatalysis applications: Modification and hybridization. *Chin. J. Catal.* 43, 2057–2090.
 9. Ghidiu, M., Lukatskaya, M.R., Zhao, M.-Q., Gogotsi, Y., and Barsoum, M.W. (2014). Conductive two-dimensional titanium carbide ‘clay’ with high volumetric capacitance. *Nature* 516, 78–81.
 10. Naguib, M., Mashitalir, O., Carle, J., Presser, V., Lu, J., Hultman, L., Gogotsi, Y., and Barsoum, M.W. (2012). Two-dimensional transition metal carbides. *ACS Nano* 6, 1322–1331.
 11. Urbankowski, P., Anasori, B., Makaryan, T., Er, D., Kota, S., Walsh, P.L., Zhao, M., Shenoy, V.B., Barsoum, M.W., and Gogotsi, Y. (2016). Synthesis of two-dimensional titanium nitride Ti_4N_3 (MXene). *Nanoscale* 8, 11385–11391.
 12. Halim, J., Kota, S., Lukatskaya, M.R., Naguib, M., Zhao, M.-Q., Moon, E.J., Pitock, J., Nanda, J., May, S.J., Gogotsi, Y., and Barsoum, M.W. (2016). Synthesis and characterization of 2D molybdenum carbide (MXene). *Adv. Funct. Mater.* 26, 3118–3127.
 13. Mashitalir, O., Lukatskaya, M.R., Zhao, M.-Q., Barsoum, M.W., and Gogotsi, Y. (2015). Amine-assisted delamination of Nb_2C MXene for Li-Ion energy storage devices. *Adv. Mater.* 27, 3501–3506.
 14. Yang, J., Naguib, M., Ghidiu, M., Pan, L.-M., Gu, J., Nanda, J., Halim, J., Gogotsi, Y., Barsoum, M.W., and Zhou, Y. (2016). Two-dimensional Nb-based M_4C_3 solid solutions (MXenes). *J. Am. Ceram. Soc.* 99, 660–666.
 15. Dall’Agnese, Y., Taberna, P.-L., Gogotsi, Y., and Simon, P. (2015). Two-dimensional vanadium carbide (MXene) as positive electrode for sodium-ion capacitors. *J. Phys. Chem. Lett.* 6, 2305–2309.
 16. Zhou, J., Palisaitis, J., Halim, J., Dahlqvist, M., Tao, Q., Persson, I., Hultman, L., Persson, P.O.Å., and Rosen, J. (2021). Boridene: Two-dimensional $\text{Mo}_{4/3}\text{B}_{2-x}$ with ordered metal vacancies obtained by chemical exfoliation. *Science* 373, 801–805.
 17. Perera, A.A.P.R., Madhushani, K.A.U., Punchihewa, B.T., Kumar, A., and Gupta, R.K. (2023). MXene-based nanomaterials for multifunctional applications. *Materials* 16, 1138.
 18. Ponnada, S., Kiai, M.S., Gorle, D.B., Bose, R.S.C., Rajagopal, V., Saini, B., Kathiresan, M., Nowduri, A., Singhal, R., Marken, F., et al. (2022). Recent status and challenges in multifunctional electrocatalysis based on 2D MXenes. *Catal. Sci. Technol.* 12, 4413–4441.
 19. Ampong, D.N., Agyekum, E., Agyemang, F.O., Mensah-Darkwa, K., Andrews, A., Kumar, A., and Gupta, R.K. (2023). MXene: fundamentals to applications in electrochemical energy storage. *Discov. Nano* 18, 3.
 20. Ajmal, Z., Qadeer, A., Khan, U., Bilal Hussain, M., Irfan, M., Mehmood, R., Abid, M., Djellabi, R., Kumar, A., Ali, H., et al. (2023). Current progresses in two-dimensional MXene-based framework: prospects from superficial synthesis to energy conversion and storage applications. *Mater. Today Chem.* 27, 101238.
 21. Ling, Z., Ren, C.E., Zhao, M.Q., Yang, J., Giannarco, J.M., Qiu, J., Barsoum, M.W., and Gogotsi, Y. (2014). Flexible and conductive MXene films and nanocomposites with high capacitance. *Proc. Natl. Acad. Sci. USA* 111, 16676–16681.
 22. Wu, X., Wang, Z., Yu, M., Xiu, L., and Qiu, J. (2017). Stabilizing the MXenes by carbon nanoploting for developing hierarchical nanohybrids with efficient lithium storage and hydrogen evolution capability. *Adv. Mater.* 29, 1607017.
 23. Wu, X., Zhou, S., Wang, Z., Liu, J., Pei, W., Yang, P., Zhao, J., and Qiu, J. (2019). Engineering multifunctional collaborative catalytic interface enabling efficient hydrogen evolution in all pH range and seawater. *Adv. Energy Mater.* 9, 1901333.
 24. Yu, M., Wang, Z., Liu, J., Sun, F., Yang, P., and Qiu, J. (2019). A hierarchically porous and hydrophilic 3D nickel-iron/MXene electrode for accelerating oxygen and hydrogen evolution at high current densities. *Nano Energy* 63, 103880.
 25. Wang, C., Chen, S., and Song, L. (2020). Tuning 2D MXenes by surface controlling and interlayer engineering: methods, properties, and synchrotron radiation characterizations. *Adv. Funct. Mater.* 30, 200869.
 26. Wei, Y., Zhang, P., Soomro, R.A., Zhu, Q., and Xu, B. (2021). Advances in the synthesis of 2D MXenes. *Adv. Mater.* 33, 2103148.
 27. Peng, J., Chen, X., Ong, W.-J., Zhao, X., and Li, N. (2019). Surface and heterointerface engineering of 2D MXenes and their nanocomposites: insights into electro- and photocatalysis. *Chem* 5, 18–50.
 28. Lukatskaya, M.R., Mashitalir, O., Ren, C.E., Dall’Agnese, Y., Rozier, P., Taberna, P.L., Naguib, M., Simon, P., Barsoum, M.W., and Gogotsi, Y. (2013). Cation intercalation and high volumetric capacitance of two-dimensional titanium carbide. *Science* 341, 1502–1505.
 29. Pang, J., Mendes, R.G., Bachmatiuk, A., Zhao, L., Ta, H.O., Gemming, T., Liu, H., Liu, Z., and Rummeli, M.H. (2019). Applications of 2D MXenes in energy conversion and storage systems. *Chem. Soc. Rev.* 48, 72–133.
 30. Miranda, A., Halim, J., Barsoum, M.W., and Lorko, A. (2016). Electronic properties of freestanding $\text{Ti}_3\text{C}_2\text{T}_x$ MXene monolayers. *Appl. Phys. Lett.* 108, 033102.
 31. Velusamy, D.B., El-Demellawi, J.K., El-Zohry, A.M., Giugni, A., Lopatin, S., Hedhili, M.N., Mansour, A.E., Fabrizio, E.D., Mohammed, O.F., and Alshareef, H.N. (2019). MXenes for plasmonic photodetection. *Adv. Mater.* 31, 1807658.
 32. Schultz, T., Frey, N.C., Hantanasirisakul, K., Park, S., May, S.J., Shenoy, V.B., Gogotsi, Y., and Koch, N. (2019). Surface termination dependent work function and electronic properties of $\text{Ti}_3\text{C}_2\text{T}_x$ MXene. *Chem. Mater.* 31, 6590–6597.
 33. Wang, Y., Nian, Y., Biswas, A.N., Li, W., Han, Y., and Chen, J.G. (2021). Challenges and opportunities in utilizing MXenes of carbides and nitrides as electrocatalysts. *Adv. Energy Mater.* 11, 2002967.
 34. Gao, Q., Feng, M., Li, E., Liu, C., Shen, C., and Liu, X. (2020). Mechanical, thermal, and rheological properties of $\text{Ti}_3\text{C}_2\text{T}_x$ MXene/thermoplastic polyurethane nanocomposites. *Macromol. Mater. Eng.* 305, 2000343.
 35. Luo, J., Wang, C., Wang, H., Hu, X., Matios, E., Lu, X., Zhang, W., Tao, X., and Li, W. (2019). Pillared MXene with ultralarge interlayer spacing as a stable matrix for high performance sodium metal anodes. *Adv. Funct. Mater.* 29, 1805946.
 36. Zhao, M.-Q., Ren, C.E., Ling, Z., Lukatskaya, M.R., Zhang, C., Van Aken, K.L., Barsoum, M.W., and Gogotsi, Y. (2015). Flexible MXene/carbon nanotube composite paper with high volumetric capacitance. *Adv. Mater.* 27, 339–345.
 37. Yan, J., Ren, C.E., Maleski, K., Hatter, C.B., Anasori, B., Urbankowski, P., Sarycheva, A., and Gogotsi, Y. (2017). Flexible MXene/graphene films for ultrafast supercapacitors with outstanding volumetric capacitance. *Adv. Funct. Mater.* 27, 1701264.
 38. Xiu, L., Wang, Z., Yu, M., Wu, X., and Qiu, J. (2018). Aggregation-resistant 3D MXene-based architecture as efficient bifunctional electrocatalyst for overall water splitting. *ACS Nano* 12, 8017–8028.
 39. Zhao, M.Q., Xie, X., Ren, C.E., Makaryan, T., Anasori, B., Wang, G., and Gogotsi, Y. (2017). Hollow MXene spheres and 3D macroporous MXene frameworks for Na-ion storage. *Adv. Mater.* 29, 1702410.
 40. Song, J., Guo, X., Zhang, J., Chen, Y., Zhang, C., Luo, L., Wang, F., and Wang, G. (2019). Rational design of free-standing 3D porous MXene/rGO hybrid aerogels as polysulfide reservoirs for high-energy lithium-sulfur batteries. *J. Mater. Chem. A* 7, 6507–6513.
 41. Ma, Y., Yue, Y., Zhang, H., Cheng, F., Zhao, W., Rao, J., Luo, S., Wang, J., Jiang, X., Liu, Z., et al. (2018). 3D synergistical MXene/reduced graphene oxide aerogel for a piezoresistive sensor. *ACS Nano* 12, 3209–3216.
 42. Yue, Y., Liu, N., Ma, Y., Wang, S., Liu, W., Luo, C., Zhang, H., Cheng, F., Rao, J., Hu, X., et al. (2018). Highly self-healable 3D microsupercapacitor with MXene-graphene composite aerogel. *ACS Nano* 12, 4224–4232.
 43. Wang, Z., Zhang, N., Yu, M., Liu, J., Wang, S., and Qiu, J. (2019). Boosting redox activity on MXene-induced multifunctional collaborative interface in high Li₂S loading cathode for high-energy Li-S and metallic Li-free rechargeable batteries. *J. Energy Chem.* 37, 183–191.
 44. Liu, J., Zhang, H.-B., Xie, X., Yang, R., Liu, Z., Liu, Y., and Yu, Z.-Z. (2018). Multifunctional, superelastic, and lightweight MXene/polymide aerogels. *Small* 14, 1802479.

45. Deng, Y., Shang, T., Wu, Z., Tao, Y., Luo, C., Liang, J., Han, D., Lyu, R., Qi, C., Lv, W., et al. (2019). Fast gelation of $Ti_3C_2T_x$ MXene initiated by metal ions. *Adv. Mater.* 31, 1902432.
46. Shi, S., Qian, B., Wu, X., Sun, H., Wang, H., Zhang, H.-B., Yu, Z.-Z., and Russell, T.P. (2019). Self-assembly of MXene-surfactants at liquid-liquid interfaces: from structured liquids to 3D aerogels. *Angew. Chem. Int. Ed.* 58, 18171–18176.
47. Wang, X., Fu, Q., Wen, J., Ma, X., Zhu, C., Zhang, X., and Qi, D. (2018). 3D $Ti_3C_2T_x$ aerogels with enhanced surface area for high performance supercapacitors. *Nanoscale* 10, 20828–20835.
48. Yang, W., Yang, J., Byun, J.J., Moissinac, F.P., Xu, J., Haigh, S.J., Domingos, M., Bissett, M.A., Dryfe, R.A.W., and Barg, S. (2019). 3D printing of freestanding MXene architectures for current-collector-free supercapacitors. *Adv. Mater.* 31, 1902725.
49. Xiao, Z., Yang, Z., Li, Z., Li, P., and Wang, R. (2019). Synchronous gains of areal and volumetric capacities in lithium-sulfur batteries promised by flower-like porous $Ti_3C_2T_x$ matrix. *ACS Nano* 13, 3404–3412.
50. Ming, F., Liang, H., Zhang, W., Ming, J., Lei, Y., Emwas, A.-H., and Alshareef, H.N. (2019). Porous MXenes enable high performance potassium ion capacitors. *Nano Energy* 62, 853–860.
51. Ren, C.E., Zhao, M.-Q., Makaryan, T., Halim, J., Boota, M., Kota, S., Anasori, B., Barsoum, M.W., and Gogotsi, Y. (2016). Porous two-dimensional transition metal carbide (MXene) flakes for high-performance Li-ion storage. *Chemelectrochem* 3, 689–693.
52. Lv, Z., Ma, W., Wang, M., Dang, J., Jian, K., Liu, D., and Huang, D. (2021). Co-conducting interfaces of multiheterostructure on MXene ($Ti_3C_2T_x$)-modified 3D self-supporting electrode for ultraefficient electrocatalytic HER in alkaline media. *Adv. Funct. Mater.* 31, 2102576.
53. Yu, M., Zheng, J., and Guo, M. (2022). La-doped NiFe-LDH coupled with hierarchical vertically aligned MXene frameworks for efficient overall water splitting. *J. Energy Chem.* 70, 472–479.
54. Yoon, Y., Tiwari, A.P., Choi, M., Novak, T.G., Song, W., Chang, H., Zyung, T., Lee, S.S., Jeon, S., and An, K.-S. (2019). Precious-metal-free electrocatalysts for activation of hydrogen evolution with nonmetallic electron donor: chemical composition controllable phosphorous doped vanadium carbide MXene. *Adv. Funct. Mater.* 29, 1903443.
55. Du, C.F., Sun, X., Yu, H., Liang, Q., Dinh, K.N., Zheng, Y., Luo, Y., Wang, Z., and Yan, Q. (2019). Synergy of Nb doping and surface alloy enhanced on water-alkali electrocatalytic hydrogen generation performance in Ti-based MXene. *Adv. Sci.* 6, 1900116.
56. Du, X., Huang, J., Zhang, J., Yan, Y., Wu, C., Hu, Y., Yan, C., Lei, T., Chen, W., Fan, C., and Xiong, J. (2019). Modulating electronic structures of inorganic nanomaterials for efficient electrocatalytic water splitting. *Angew. Chem. Int. Ed.* 58, 4484–4502.
57. Kuznetsov, D.A., Chen, Z., Kumar, P.V., Tsoukalou, A., Kierzkowska, A., Abdala, P.M., Safanova, O.V., Fedorov, A., and Müller, C.R. (2019). Single site cobalt substitution in 2D molybdenum carbide (MXene) enhances catalytic activity in the hydrogen evolution reaction. *J. Am. Chem. Soc.* 141, 17809–17816.
58. VahidMohammadi, A., Rosen, J., and Gogotsi, Y. (2021). The world of two-dimensional carbides and nitrides (MXenes). *Science* 372, 1165.
59. Zhan, X., Si, C., Zhou, J., and Sun, Z. (2020). MXene and MXene-based composites: synthesis, properties and environment-related applications. *Nanoscale Horiz.* 5, 235–258.
60. Ma, T.Y., Cao, J.L., Jaroniec, M., Qiao, S.Z., and Qiao, S.Z. (2016). Interacting carbon nitride and titanium carbide nanosheets for high performance oxygen evolution. *Angew. Chem. Int. Ed.* 55, 1138–1142.
61. Zhao, L., Dong, B., Li, S., Zhou, L., Lai, L., Wang, Z., Zhao, S., Han, M., Gao, K., Lu, M., et al. (2017). Interdiffusion reaction-assisted hybridization of two-dimensional metal-organic frameworks and $Ti_3C_2T_x$ nanosheets for electrocatalytic oxygen evolution. *ACS Nano* 11, 5800–5807.
62. Li, L., Yu, D., Li, P., Huang, H., Xie, D., Lin, C.-C., Hu, F., Chen, H.-Y., and Peng, S. (2021). Interfacial electronic coupling of ultrathin transition-metal hydroxide nanosheets with layered MXenes as a new prototype for platinum-like hydrogen evolution. *Energy Environ. Sci.* 14, 6419–6427.
63. Li, Z., Qi, Z., Wang, S., Ma, T., Zhou, L., Wu, Z., Luan, X., Lin, F.-Y., Chen, M., Miller, J.T., et al. (2019). In situ formed Pt_3Ti nanoparticles on a two-dimensional transition metal carbide (MXene) used as efficient catalysts for hydrogen evolution reactions. *Nano Lett.* 19, 5102–5108.
64. Zhang, J., Zhao, Y., Guo, X., Chen, C., Dong, C.-L., Liu, R.-S., Han, C.-P., Li, Y., Gogotsi, Y., and Wang, G. (2018). Single platinum atoms immobilized on an MXene as an efficient catalyst for the hydrogen evolution reaction. *Nat. Catal.* 1, 985–992.
65. Ramalingam, V., Varadhan, P., Fu, H.-C., Kim, H., Zhang, D., Chen, S., Song, L., Ma, D., Wang, Y., Alshareef, H.N., and He, J.-H. (2019). Heteroatom-mediated interactions between ruthenium single atoms and an MXene support for efficient hydrogen evolution. *Adv. Mater.* 31, 1903841.
66. Thakur, R., VahidMohammadi, A., Moncada, J., Adams, W.R., Chi, M., Tatarchuk, B., Beidaghi, M., and Carrero, C.A. (2019). Insights into the thermal and chemical stability of multilayered V_2CT_x MXene. *Nanoscale* 11, 10716–10726.
67. Zhang, C.J., Pinilla, S., McEvoy, N., Cullen, C.P., Anasori, B., Long, E., Park, S.-H., Seral-Ascaso, A., Shmeliov, A., Krishnan, D., et al. (2017). Oxidation stability of colloidal two-dimensional titanium carbides (MXenes). *Chem. Mater.* 29, 4848–4856.
68. Rakhi, R.B., Ahmed, B., Hedhili, M.N., Anjum, D.H., and Alshareef, H.N. (2015). Effect of postetch annealing gas composition on the structural and electrochemical properties of Ti_2CT_x MXene electrodes for supercapacitor applications. *Chem. Mater.* 27, 5314–5323.
69. Chae, Y., Kim, S.J., Cho, S.-Y., Choi, J., Maleski, K., Lee, B.-J., Jung, H.-T., Gogotsi, Y., Lee, Y., and Ahn, C.W. (2019). An investigation into the factors governing the oxidation of two-dimensional Ti_3C_2 MXene. *Nanoscale* 11, 8387–8393.
70. Wang, X., Wang, Z., and Qiu, J. (2021). Stabilizing MXene by hydration chemistry in aqueous solution. *Angew. Chem. Int. Ed.* 60, 26587–26591.
71. VahidMohammadi, A., Mojtabavi, M., Caffrey, N.M., Wanunu, M., and Beidaghi, M. (2019). Assembling 2D MXenes into highly stable pseudocapacitive electrodes with high power and energy densities. *Adv. Mater.* 31, 1806931.
72. Natu, V., Hart, J.L., Sokol, M., Chiang, H., Taheri, M.L., and Barsoum, M.W. (2019). Edge capping of 2D-MXene sheets with polyanionic salts to mitigate oxidation in aqueous colloidal suspensions. *Angew. Chem. Int. Ed.* 58, 12655–12660.
73. Zhao, X., Vashisth, A., Prehn, E., Sun, W., Shah, S.A., Habib, T., Chen, Y., Tan, Z., Lutkenhaus, J.L., Radovic, M., and Green, M.J. (2019). Antioxidants unlock shelf-stable Ti_3C_2T (MXene) nanosheet dispersions. *Matter* 1, 513–526.
74. Lee, Y., Kim, S.J., Kim, Y.-J., Lim, Y., Chae, Y., Lee, B.-J., Kim, Y.-T., Han, H., Gogotsi, Y., and Ahn, C.W. (2020). Oxidation-resistant titanium carbide MXene films. *J. Mater. Chem. A* 8, 573–581.
75. Zhang, J., Kong, N., Hegh, D., Usman, K.A.S., Guan, G., Qin, S., Jurewicz, I., Yang, W., and Razal, J.M. (2020). Freezing titanium carbide aqueous dispersions for ultra-long-term storage. *ACS Appl. Mater. Interfaces* 12, 34032–34040.
76. Fang, Y., Liu, Z., Han, J., Jin, Z., Han, Y., Wang, F., Niu, Y., Wu, Y., and Xu, Y. (2019). High-performance electrocatalytic conversion of N_2 to NH_3 using oxygen-vacancy-rich TiO_2 in situ grown on $Ti_3C_2T_x$ MXene. *Adv. Energy Mater.* 9, 1803406.
77. Lim, K.R.G., Handoko, A.D., Johnson, L.R., Meng, X., Lin, M., Subramanian, G.S., Anasori, B., Gogotsi, Y., Vojvodic, A., and Seh, Z.W. (2020). 2H- Mo_2S_2 on Mo_2CT_x MXene nanohybrid for efficient and durable electrocatalytic hydrogen evolution. *ACS Nano* 14, 16140–16155.
78. Tang, J., Mathis, T.S., Kurra, N., Sarycheva, A., Xiao, X., Hedhili, M.N., Jiang, Q., Alshareef, H.N., Xu, B., Pan, F., et al. (2019). Tuning the electrochemical performance of titanium carbide MXene by controllable in situ anodic oxidation. *Angew. Chem. Int. Ed.* 58, 17849–17855.
79. Dong, Y., Wu, Z.-S., Zheng, S., Wang, X., Qin, J., Wang, S., Shi, X., and Bao, X. (2017). Ti_2C_2 MXene-derived sodium/potassium titanate nanoribbons for high-performance sodium/potassium ion batteries with enhanced capacities. *ACS Nano* 11, 4792–4800.
80. Jiao, L., Zhang, C., Geng, C., Wu, S., Li, H., Lv, W., Tao, Y., Chen, Z., Zhou, G., Li, J., et al. (2019). Capture and catalytic conversion of polysulfides by in situ built TiO_2 -MXene heterostructures for lithium-sulfur batteries. *Adv. Energy Mater.* 9, 1900219.
81. Liu, S., Wang, Z., Zhou, S., Yu, F., Yu, M., Chiang, C.Y., Zhou, W., Zhao, J., and Qiu, J. (2017). Metal-organic-framework-derived hybrid carbon nanocages as a bifunctional electrocatalyst for oxygen reduction and evolution. *Adv. Mater.* 29, 1700874.
82. Li, Z., Zhuang, Z., Lv, F., Zhu, H., Zhou, L., Luo, M., Zhu, J., Lang, Z., Feng, S., Chen, W., et al. (2018). The marriage of the FeN_4 moiety and MXene boosts oxygen reduction catalysis: Fe 3d electron delocalization matters. *Adv. Mater.* 30, 1803220.
83. Wu, Z., Wang, H., Xiong, P., Li, G., Qiu, T., Gong, W.-B., Zhao, F., Li, C., Li, Q., Wang,

- G., and Geng, F. (2020). Molecularly thin nitride sheets stabilized by titanium carbide as efficient bifunctional electrocatalysts for fiber-shaped rechargeable zinc-air batteries. *Nano Lett.* 20, 2892–2898.
84. Kuznetsov, D.A., Chen, Z., Abdala, P.M., Safonova, O.V., Fedorov, A., and Müller, C.R. (2021). Single-atom-substituted $\text{Mo}_2\text{CT}_x/\text{Fe}$ -layered carbide for selective oxygen reduction to hydrogen peroxide: tracking the evolution of the MXene phase. *J. Am. Chem. Soc.* 143, 5771–5778.
85. Yu, M., Zhou, S., Wang, Z., Zhao, J., and Qiu, J. (2018). Boosting electrocatalytic oxygen evolution by synergistically coupling layered double hydroxide with MXene. *Nano Energy* 44, 181–190.
86. Zhang, Y., Jiang, H., Lin, Y., Liu, H., He, Q., Wu, C., Duan, T., and Song, L. (2018). In situ growth of cobalt nanoparticles encapsulated nitrogen-doped carbon nanotubes among $\text{Ti}_3\text{C}_2\text{T}_x$ (MXene) matrix for oxygen reduction and evolution. *Adv. Mater. Interfaces* 5, 1800392.
87. Ashton, M., Trometer, N., Mathew, K., Suntivich, J., Freysoldt, C., Sinnott, S.B., and Hennig, R.G. (2019). Predicting the electrochemical synthesis of 2D materials from first principles. *J. Phys. Chem. C* 123, 3180–3187.
88. Lagadec, M.F., and Grimaud, A. (2020). Water electrolyzers with closed and open electrochemical systems. *Nat. Mater.* 19, 1140–1150.
89. Jin, H., Yu, H., Li, H., Davey, K., Song, T., Paik, U., and Qiao, S.Z. (2022). MXene analogue: a 2D nitridene solid solution for high-rate hydrogen production. *Angew. Chem. Int. Ed.* 61, e202203850.
90. Wang, L., Hao, Y., Deng, L., Hu, F., Zhao, S., Li, L., and Peng, S. (2022). Rapid complete reconfiguration induced actual active species for industrial hydrogen evolution reaction. *Nat. Commun.* 13, 5785.
91. Wang, X., Ding, J., Song, W., Yang, X., Zhang, T., Huang, Z., Wang, H., Han, X., and Hu, W. (2023). Cation vacancy clusters in $\text{Ti}_3\text{C}_2\text{T}_x$ MXene induce ultra-strong interaction with noble metal clusters for efficient electrocatalytic hydrogen evolution. *Adv. Energy Mater.* 13, 2300148.
92. Cui, C., Cheng, R., Zhang, H., Zhang, C., Ma, Y., Shi, C., Fan, B., Wang, H., and Wang, X. (2020). Ultrastable MXene@Pt/SWCNTs' nanocatalysts for hydrogen evolution reaction. *Adv. Funct. Mater.* 30, 2000693.
93. Zou, Y., Kazemi, S.A., Shi, G., Liu, J., Yang, Y., Bedford, N.M., Fan, K., Xu, Y., Fu, H., Dong, M., et al. (2023). Ruthenium single-atom modulated $\text{Ti}_3\text{C}_2\text{T}_x$ MXene for efficient alkaline electrocatalytic hydrogen production. *Ecomat* 5, e12274.
94. Li, K., Liang, M., Wang, H., Wang, X., Huang, Y., Coelho, J., Pinilla, S., Zhang, Y., Qi, F., Nicolosi, V., and Xu, Y. (2020). 3D MXene architectures for efficient energy storage and conversion. *Adv. Funct. Mater.* 30, 2000842.
95. Xiu, L., Pei, W., Zhou, S., Wang, Z., Yang, P., Zhao, J., and Qiu, J. (2020). Multilevel hollow MXene tailored low-Pt catalyst for efficient hydrogen evolution in full-pH range and seawater. *Adv. Funct. Mater.* 30, 1910028.
96. Ajmal, S., Kumar, A., Selvaraj, M., Alam, M.M., Yang, Y., Das, D.K., Gupta, R.K., and Yasin, G. (2023). MXenes and their interfaces for the taming of carbon dioxide & nitrate: A critical review. *Coord. Chem. Rev.* 483, 215094.
97. Li, F., Ai, H., Shi, C., Lo, K.H., and Pan, H. (2021). Single transition metal atom catalysts on Ti_2CN_2 for efficient CO_2 reduction reaction. *Int. J. Hydrogen Energy* 46, 12886–12896.
98. Hao, Y., Hu, F., Zhu, S., Sun, Y., Wang, H., Wang, L., Wang, Y., Xue, J., Liao, Y.F., Shao, M., and Peng, S. (2023). MXene-regulated metal-oxide interfaces with modified intermediate configurations realizing nearly 100% CO_2 electrocatalytic conversion. *Angew. Chem. Int. Ed.* 62, e202304179.
99. Abdinejad, M., Subramanian, S., Motlagh, M.K., Noroozifar, M., Duangdangchote, S., Neoporozhni, I., Ripepi, D., Pinto, D., Li, M., Tang, K., et al. (2023). Insertion of MXene-based materials into Cu-Pd 3D aerogels for electroreduction of CO_2 to formate. *Adv. Energy Mater.* 13, 2300402.
100. Handoko, A.D., Chen, H., Lum, Y., Zhang, Q., Anasori, B., and Seh, Z.W. (2020). Two-dimensional titanium and molybdenum carbide MXenes as electrocatalysts for CO_2 reduction. *iScience* 23, 101181.
101. Handoko, A.D., Khoo, K.H., Tan, T.L., Jin, H., and Seh, Z.W. (2018). Establishing new scaling relations on two-dimensional MXenes for CO_2 electroreduction. *J. Mater. Chem. A* 6, 21885–21890.
102. Wang, S., Li, L., San Hui, K., Bin, F., Zhou, W., Fan, X., Zalnezhad, E., Li, J., and Hui, K.N. (2021). Computational screening of single atoms anchored on defective Mo_2CO_2 MXene nanosheet as efficient electrocatalysts for the synthesis of ammonia. *Adv. Eng. Mater.* 23, 2100405.
103. Chu, K., Luo, Y., Shen, P., Li, X., Li, Q., and Guo, Y. (2022). Unveiling the synergy of O-vacancy and heterostructure over MoO_3 / MXene for N_2 electroreduction to NH_3 . *Adv. Energy Mater.* 12, 2103022.
104. Johnson, L.R., Sridhar, S., Zhang, L., Fredrickson, K.D., Raman, A.S., Jang, J., Leach, C., Padmanabhan, A., Price, C.C., Frey, N.C., et al. (2020). MXene materials for the electrochemical nitrogen reduction-functionalized or not? *ACS Catal.* 10, 253–264.
105. Zhou, S., Zhao, Y., Shi, R., Wang, Y., Ashok, A., Héraly, F., Zhang, T., and Yuan, J. (2022). Vacancy-rich MXene-immobilized Ni single atoms as a high-performance electrocatalyst for the hydrazine oxidation reaction. *Adv. Mater.* 34, 2204388.
106. Sun, F., Qin, J., Wang, Z., Yu, M., Wu, X., Sun, X., and Qiu, J. (2021). Energy-saving hydrogen production by chlorine-free hybrid seawater splitting coupling hydrazine degradation. *Nat. Commun.* 12, 4182.
107. Abbott, D.F., Xu, Y.Z., Kuznetsov, D.A., Kumar, P., Müller, C.R., Fedorov, A., and Mougel, V. (2023). Understanding the synergy between Fe and Mo sites in the nitrate reduction reaction on a bio-inspired bimetallic MXene electrocatalyst. *Angew. Chem. Int. Ed.* 62, e202313746.
108. Ren, Y., Tian, F., Jin, L., Wang, Y., Yang, J., You, S., and Liu, Y. (2023). Fluidic MXene Electrode Functionalized with Iron Single Atoms for Selective Electrocatalytic Nitrate Transformation to Ammonia. *Environ. Sci. Technol.* 57, 10458–10466.
109. Zhang, L., Wang, Z., and Qiu, J. (2022). Energy-saving hydrogen production by seawater electrolysis coupling sulfion degradation. *Adv. Mater.* 34, e2109321.
110. Ma, Q., Gao, J., Moussa, B., Young, J., Zhao, M., and Zhang, W. (2023). Electrosorption, desorption, and oxidation of perfluoroalkyl carboxylic acids (PFCAs) via MXene-based electrocatalytic membranes. *ACS Appl. Mater. Interfaces* 15, 29149–29159.
111. Pang, S.Y., Io, W.F., Wong, L.W., Zhao, J., and Hao, J. (2020). Efficient energy conversion and storage based on robust fluoride-free self-assembled 1D niobium carbide in 3D nanowire network. *Adv. Sci.* 7, 1903680.
112. Shen, M., Jiang, W., Liang, K., Zhao, S., Tang, R., Zhang, L., and Wang, J.Q. (2021). One-pot green process to synthesize MXene with controllable surface terminations using molten salts. *Angew. Chem. Int. Ed.* 60, 27013–27018.
113. Li, Y., Shao, H., Lin, Z., Lu, J., Liu, L., Dupoyer, B., Persson, P.O.Å., Eklund, P., Hultman, L., Li, M., et al. (2020). A general Lewis acidic etching route for preparing MXenes with enhanced electrochemical performance in non-aqueous electrolyte. *Nat. Mater.* 19, 894–899.
114. Chen, N., Duan, Z., Cai, W., Wang, Y., Pu, B., Huang, H., Xie, Y., Tang, Q., Zhang, H., and Yang, W. (2023). Supercritical etching method for the large-scale manufacturing of MXenes. *Nano Energy* 107, 108147.
115. Sun, Y., and Dai, S. (2021). High-entropy materials for catalysis: a new frontier. *Sci. Adv.* 7, eabg1600.
116. Wang, Y., Mi, J., and Wu, Z.-S. (2022). Recent status and challenging perspective of high entropy oxides for chemical catalysis. *Chem. Catal.* 2, 1624–1656.
117. Du, Z., Wu, C., Chen, Y., Cao, Z., Hu, R., Zhang, Y., Gu, J., Cui, Y., Chen, H., Shi, Y., et al. (2021). High-entropy atomic layers of transition-metal carbides (MXenes). *Adv. Mater.* 33, 2101473.
118. Nemani, S.K., Zhang, B., Wyatt, B.C., Hood, Z.D., Manna, S., Khaledaliidusti, R., Hong, W., Sternberg, M.G., Sankaranarayanan, S.K.R.S., and Anasori, B. (2021). High-entropy 2D carbide MXenes: TiVnBMoC_3 and TiVCrMoC_3 . *ACS Nano* 15, 12815–12825.
119. Zhu, X., Zhou, X., Jing, Y., and Li, Y. (2021). Electrochemical synthesis of urea on MBenes. *Nat. Commun.* 12, 4080.
120. Zhang, T., Zhang, B., Peng, Q., Zhou, J., and Sun, Z. (2021). Mo_2B_2 MBene-supported single-atom catalysts as bifunctional HER/OER and OER/ORR electrocatalysts. *J. Mater. Chem. A* 9, 433–441.
121. Vijayaprabhakaran, A., and Kathiresan, M. (2023). Fluorine-free synthesized tantalum carbide (Ta_2C MXene) as an efficient electrocatalyst for water reduction and nitro compound reduction. *Mater. Adv.* 4, 3593–3602.
122. Luo, Y., Zhang, Z., Chhowalla, M., and Liu, B. (2022). Recent advances in design of electrocatalysts for high-current-density water splitting. *Adv. Mater.* 34, e2108133.